J Sci Comput (2016) 68:143–170
DOI 10.1007/s10915-015-0132-2

Stability Analysis of Discontinuous Galerkin Approximations to the Elastodynamics Problem

Paola F. Antonietti[5] · **Blanca Ayuso de Dios**[2,3,4] · **Ilario Mazzieri**[5] · **Alfio Quarteroni**[1,5]

Received: 18 May 2015 / Revised: 1 November 2015 / Accepted: 5 November 2015 /
Published online: 21 November 2015

Abstract We consider semi-discrete discontinuous Galerkin approximations of both *displacement* and *displacement-stress* formulations of the elastodynamics problem. We prove the stability analysis in the natural energy norm and derive optimal a-priori error estimates. For the *displacement-stress* formulation, schemes preserving the total energy of the system are introduced and discussed. We verify our theoretical estimates on two and three dimensions test problems.

Keywords Discontinuous Galerkin methods · Elastodynamics equation · Stability and error analysis

Blanca Ayuso de Dios is on leave from the Instituion which is in Affiliation 4. Alfio Quarteroni is on leave from the Institution which is in Affiliation 5.

✉ Ilario Mazzieri
ilario.mazzieri@polimi.it

Paola F. Antonietti
paola.antonietti@polimi.it

Blanca Ayuso de Dios
blanca.ayuso@tuhh.de; blanca@imati.cnr.it

Alfio Quarteroni
alfio.quarteroni@epfl.ch

1 CMCS, Ecole Polytechnique Federale de Lausanne (EPFL), Station 8, 1015 Lausanne, Switzerland

2 Institut für Mathematik, Technische Universität Hamburg-Harburg, Am Schwarzenberg-Campus 3, 21073 Hamburg, Germany

3 Istituto di Matematica Applicata e Tecnologie Informatiche (IMATI) – CNR, 27100 Pavia, Italy

4 Dipartimento di Matematica, Università di Bologna, Piazza di Porta San Donato 5, 40126 Bologna, Italy

5 MOX, Dipartimento di Matematica, Politecnico di Milano, Piazza Leonardo da Vinci 32, 20133 Milan, Italy

Mathematics Subject Classification 65M12 · 65M60

1 Introduction

The purpose of this paper is to design and analyze semi-discrete discontinuous Galerkin (DG) methods for a general elastodynamics problem. The use of the elastodynamics equation to model the seismic response of heterogeneous media with irregular topography and complex physical layers is a subject of research that has been intensively investigated in recent years. Thanks to the advances in computer facilities, the development of numerical methods for seismic wave propagation has found relevant applications and is currently a very active research field. The most employed numerical strategies for seismic modelling include finite difference (FD), pseudo-spectral (PS), and (continuous and discontinuous) spectral element (SE) methods, see, e.g. [12,27,38,51] and the references therein. In particular, for earthquake modelling a large number of FD schemes have been developed so far. Such schemes may considerably differ form each other either in methodological and algorithmic aspects. In some special configurations the most advanced FD schemes can be as competitive as PS and SE methods: for the same level of accuracy, they can be even more computationally efficient. However, whenever geometrically and rheologically complex realistic problems are considered, FD methods are lacking in efficiency, see [38] for a comprehensive review. Fourier PS methods have been originally introduced in [32], and combine the simplicity of the spatial discretization on a structured grid with the optimal accuracy of global spectral differential operators. If on one hand PS methods retain an unbeatable low spatial sampling ratio and computational efficiency, on the other hand they face accuracy problems when modelling seismic wave propagation in media with sharp velocity contrasts [37] and free-surface boundary conditions [53]. Moreover, the expensive interprocessor communication required by the algorithm undermine their parallel efficiency, although some remedies have been proposed in [27] to alleviate the above mentioned shortcomings, making PS acceptable for complex earthquake simulations. After more than twenty year since their first application in fluid dynamics [41], continuous SE methods have become one of the most effective and powerful approaches for solving three-dimensional seismic wave propagation problems in highly heterogeneous media, the first applications in elastodynamics can be found in [19,30,48]. The geometrical flexibility (inherited from finite element methods), the high order accuracy (acquired from spectral methods) and the native orientation towards high performance parallel computing are some of the most important properties featured by SE schemes. Relevant applications in computational seismology are presented in [29,36,50]. However, the use of a uniform polynomial order on the whole computational domain typical of continuous SE can lead to an unreasonably large computational effort, in particular whenever a fine mesh grid is already needed to describe accurately the computational domain. The flexibility of high-order/SE Discontinuous Galerkin methods [3,4,25] can further improve the capabilities of SE discretizations and make them very well suited to deal with (i) the intrinsic multi-scale nature of seismic wave propagation problems, involving a relative broad range of wavelengths; (ii) the complexity of the geometric constraints while keeping the computational effort low, see e.g. [35].

So far, two main streams have been followed in the design and analysis of DG methods for elastodynamics: the *displacement* formulation and the *velocity-stress* formulation. For the former, DG methods of Interior Penalty (IP) type, symmetric and non-symmetric, have been proposed and analyzed in [45,47] for the approximation of acoustic and elastic wave equations. These schemes have been extended to Spectral-DG methods in [4], to DG approximations of viscoelasticity in [46] and to nonlinear elastodynamics in [39]. For the

velocity-stress formulations, the design of DG methods follow the traditional guidelines of DG schemes for hyperbolic conservation laws. In this regard, conservative methods based on the use of central fluxes have been proposed in [17], while non-conservative methods based on upwinding fluxes are studied in [26]. The DG method developed in [52] is based on a velocity-strain formulation of the coupled elastic-acoustic wave equations; this allows the acoustic and elastic wave equations to be expressed in conservative form within the same framework.

Here, we introduce a fairly general family of semidiscrete DG methods for both the *displacement* and *displacement-stress* formulations of the elastodynamics problem with mixed boundary conditions (those typically encountered in seismic applications) and the main goal is to identify the key ingredients to ensure stability of the methods. For this reason, we start with the *displacement-stress* formulations which gives further insight on the features required by the methods. Finite Element methods for the *displacement-stress* formulation were proposed and analyzed in the seminal work [33] (see also [34]). Here, some extra difficulties arise in the analysis due to the discontinuous nature of the spaces and the fact that we consider the general problem with mixed boundary conditions. However, the flexibility of DG framework allow us to construct in a simple way, *displacement-stress* DG methods that are fully conservative (in the sense that the total discrete energy is preserved). For the *displacement* formulation, we consider Interior Penalty (IP) schemes, focusing on symmetric methods, similar to those considered for wave equation in [22], but different from the IP schemes introduced in [45–47] for linear elastodynamics and those used in [39] for nonlinear elastodynamics. The IP methods considered in those works contain an extra term that penalizes the time derivative of the displacement besides the displacement itself. This term was required to allow for the stability analysis. However, as we shall demonstrate via numerical experiments, the inclusion of such an extra term, seems to undermine the overall stability. Here, we prove stability in the natural energy norm associated to the symmetric IP methods, with no extra stabilization terms.

As a product of the stability analysis, we obtain optimal error estimates for all the considered DG schemes. Our semidiscrete analysis represents an intermediate but essential step to derive the fully discrete stability analysis after discretization in space. The analysis of the fully discrete schemes is out of the scope of the present paper and will be subject of future work.

The paper is organized as follows. In Sect. 2 we introduce the model problem and revise some key results. The discrete notation is given in Sect. 3, while in Sect. 4 we introduce the family of DG methods. The stability analysis is presented in Sect. 5, whereas in Sect. 6 we state the *a priori* error estimates. Numerical experiments verifying the theory are presented in Sect. 7. In Sect. 8 we draw some conclusions. The paper is closed with "Appendix" containing some technical results.

Throughout the paper, we use standard notation for Sobolev spaces [1]. The Sobolev spaces of vector-valued and symmetric tensor-valued functions are denoted by $\mathbf{H}^m(D) = [H^m(D)]^d$ and $\boldsymbol{\mathcal{H}}^m(D) = [H^m(D)]^{d\times d}_{\text{sym}}$, respectively. We will use the symbol $(\cdot,\cdot)_D$ to denote the standard inner product in any of the spaces $\mathbf{H}^0(D) = \mathbf{L}^2(D)$ or $\boldsymbol{\mathcal{H}}^0(D) = \boldsymbol{\mathcal{L}}^2(D)$. C denotes a generic positive constant that may take different values in different places, but is always mesh independent. The notation $x \lesssim y$ will represent the inequality $x \leq Cy$ for a constant C as before.

2 Continuous Problem

Let $\Omega \subset \mathbb{R}^d$, $d = 2, 3$, be an open, bounded region with Lipschitz boundary $\partial\Omega$ and outward normal unit vector $\mathbf{n}$, and let $\partial\Omega$ be composed of two disjoint portions Γ_D and

Γ_N, with meas$(\Gamma_D) > 0$. Given a volume force $\mathbf{f} \in L^2((0,T];\mathbf{L}^2(\Omega))$, a boundary datum $\mathbf{g} \in C^1((0,T];\mathbf{H}^{1/2}(\Gamma_N))$, and smooth enough initial conditions $\mathbf{u}_0 \in \mathbf{H}^1_{0,\Gamma_D}(\Omega)$ and $\mathbf{u}_1 \in \mathbf{L}^2(\Omega)$, we consider the mathematical model of linear elastodynamics:

$$\rho(\mathbf{x})\mathbf{u}_{tt}(\mathbf{x},t) - \nabla\cdot\boldsymbol{\sigma}(\mathbf{x},t) = \mathbf{f}(\mathbf{x},t), \qquad \text{in } \Omega\times(0,T], \tag{1a}$$

$$\mathcal{A}\boldsymbol{\sigma}(\mathbf{x},t) - \boldsymbol{\varepsilon}(\mathbf{u}(\mathbf{x},t)) = \mathbf{0}, \qquad \text{in } \Omega\times(0,T], \tag{1b}$$

$$\mathbf{u}(\mathbf{x},t) = \mathbf{0}, \qquad \text{on } \Gamma_D\times(0,T], \tag{1c}$$

$$\boldsymbol{\sigma}(\mathbf{x},t)\mathbf{n}(\mathbf{x}) = \mathbf{g}(\mathbf{x},t), \qquad \text{on } \Gamma_N\times(0,T], \tag{1d}$$

$$\mathbf{u}_t(\mathbf{x},0) = \mathbf{u}_1(\mathbf{x}), \qquad \text{in } \Omega\times\{0\}, \tag{1e}$$

$$\mathbf{u}(\mathbf{x},0) = \mathbf{u}_0(\mathbf{x}), \qquad \text{in } \Omega\times\{0\}, \tag{1f}$$

where $\boldsymbol{\sigma} : \Omega\times[0,T] \to \mathbb{S} = \mathbb{R}^{d\times d}_{\text{sym}}$ is the Cauchy stress tensor and $\mathbf{u} : \Omega\times[0,T] \longrightarrow \mathbb{R}^d$ is the displacement vector field. The mass density $\rho \in L^\infty(\Omega)$ is a strictly positive function, i.e.,

$$0 < \rho_* \le \rho(\mathbf{x}) \le \rho^* \qquad \forall \mathbf{x}\in\Omega. \tag{2}$$

We denote by $\boldsymbol{\varepsilon}(\mathbf{u}) : \Omega \longrightarrow \mathbb{S}$ the symmetric gradient defined by $\boldsymbol{\varepsilon}(\mathbf{u}) = \frac{1}{2}(\nabla\mathbf{u} + \nabla\mathbf{u}^\top)$. The compliance tensor $\mathcal{A} = \mathcal{A}(x) : \mathbb{S} \longrightarrow \mathbb{S}$ is a bounded, symmetric and uniformly positive definite operator, encoding the material properties, such that

$$\mathcal{A}\boldsymbol{\sigma} = \frac{1}{2\mu}\left(\boldsymbol{\sigma} - \frac{\lambda}{3\lambda+2\mu}\text{tr}(\boldsymbol{\sigma})\mathbb{I}\right) \qquad \forall\,\boldsymbol{\sigma}\in\mathbb{S}\,, \tag{3}$$

where $\mathbb{I}\in\mathbb{R}^{d\times d}$ is the identity operator, tr$(\cdot)$ stands for the trace operator, and both the Lamé parameters $\lambda, \mu \in L^\infty(\Omega)$ are positive functions. Provided $\mathcal{A}$ is invertible, (3) is equivalent to the Hooke's law $\boldsymbol{\sigma} = \mathcal{A}^{-1}\boldsymbol{\varepsilon} = \mathcal{D}\boldsymbol{\varepsilon}$, with

$$\mathcal{D} : \mathbb{S} \longrightarrow \mathbb{S}, \quad \mathcal{D}\boldsymbol{\tau} = 2\mu\boldsymbol{\tau} + \lambda\text{tr}(\boldsymbol{\tau})\mathbb{I} \quad \forall\,\boldsymbol{\tau}\in\mathbb{S}\,. \tag{4}$$

In this case, from the properties of $\mathcal{A}$, it is directly inferred that $\mathcal{D}$ is symmetric, bounded and positive definite, i.e., there exist $\mathrm{D}_*, \mathrm{D}^* > 0$ such that

$$0 < \mathrm{D}_*(\boldsymbol{\tau},\boldsymbol{\tau})_\Omega \le (\mathcal{D}\boldsymbol{\tau},\boldsymbol{\tau})_\Omega \le \mathrm{D}^*(\boldsymbol{\tau},\boldsymbol{\tau})_\Omega \quad \forall\,\boldsymbol{\tau}\in\mathbb{R}^{d\times d}, \quad \boldsymbol{\tau}\neq\mathbf{0}. \tag{5}$$

To simplify the notation, in the following we will write $\mathbf{g}_0 = \mathbf{g}(\mathbf{x},0)$, $\boldsymbol{\sigma}_0 = \boldsymbol{\sigma}(\mathbf{x},0) = \mathcal{D}\boldsymbol{\varepsilon}(\mathbf{u}(\mathbf{x},0)) = \mathcal{D}\boldsymbol{\varepsilon}(\mathbf{u}_0)$.

We next consider the variational formulation of (1a)–(1f): for all $t\in(0,T]$ find $(\mathbf{u},\boldsymbol{\sigma}) \in \mathbf{H}^1_{0,\Gamma_D}(\Omega)\times\boldsymbol{\mathcal{L}}^2(\Omega)$ such that:

$$(\rho\mathbf{u}_{tt},\mathbf{v})_\Omega + (\boldsymbol{\sigma},\boldsymbol{\varepsilon}(\mathbf{v}))_\Omega = (\mathbf{f},\mathbf{v})_\Omega + (\mathbf{g},\mathbf{v})_{\Gamma_N} \qquad \forall\,\mathbf{v}\in\mathbf{H}^1_{0,\Gamma_D}(\Omega), \tag{6a}$$

$$(\mathcal{A}\boldsymbol{\sigma},\boldsymbol{\tau})_\Omega - (\boldsymbol{\varepsilon}(\mathbf{u}),\boldsymbol{\tau})_\Omega = 0 \qquad \forall\,\boldsymbol{\tau}\in\boldsymbol{\mathcal{L}}^2(\Omega). \tag{6b}$$

Under the above regularity assumptions the saddle problem (6a)–(6b) has a unique solution $(\mathbf{u},\boldsymbol{\sigma}) \in \mathbf{H}^1_{0,\Gamma_D}(\Omega)\times\boldsymbol{\mathcal{L}}^2(\Omega)$, [18], and satisfies *a priori* stability estimate in the following energy norm

$$\|(\mathbf{u}(t),\boldsymbol{\sigma}(t))\|^2_{\mathcal{E}} = \left\|\rho^{1/2}\mathbf{u}_t(t)\right\|^2_{0,\Omega} + \left\|\mathcal{A}^{1/2}\boldsymbol{\sigma}(t)\right\|^2_{0,\Omega}\,, \quad \forall\, t\in[0,T].$$

For further details we refer the reader to [18, Theorem 4.1] for the general existence result, cf. also [2, Appendix A].

Remark 1 Choosing $\boldsymbol{\tau} = \boldsymbol{\varepsilon}(\mathbf{v})$ in (6b) and substituting the result in (6a) we obtain the following equivalent weak problem: for all $t \in (0, T]$ find $\mathbf{u} \in \mathbf{H}^1_{0,\Gamma_D}(\Omega)$ such that:

$$(\rho \mathbf{u}_{tt}, \mathbf{v})_\Omega + (\mathcal{D}\boldsymbol{\varepsilon}(\mathbf{u}), \boldsymbol{\varepsilon}(\mathbf{v}))_\Omega = (\mathbf{f}, \mathbf{v})_\Omega + (\mathbf{g}, \mathbf{v})_{\Gamma_N} \qquad \forall\, \mathbf{v} \in \mathbf{H}^1_{0,\Gamma_D}(\Omega). \tag{7}$$

This problem (7) is well posed and that its unique solution satisfies $\mathbf{u} \in C((0, T]; \mathbf{H}^1_{0,\Gamma_D}(\Omega)) \cap C^1((0, T]; \boldsymbol{\mathcal{L}}^2(\Omega))$, see [44, Theorem 8-3.1].

Finally, we will often use the following integration by parts formula that holds for $\mathbf{w}, \mathbf{z} \in \mathcal{C}^1((0, T))$

$$\int_0^t (\mathbf{w}, \mathbf{z}_\tau) d\tau = (\mathbf{w}(t), \mathbf{z}(t)) - (\mathbf{w}(0), \mathbf{z}(0)) - \int_0^t (\mathbf{w}_\tau, \mathbf{z}) d\tau. \tag{8}$$

3 Notation and Technical Tools for the Discrete Approximation

In this section we introduce some notation and revise some technical tools that will be used in our analysis.

3.1 Mesh Partitions

We consider a family $\{\mathcal{T}_h, 0 < h \leq 1\}$ of shape-regular conforming partitions of Ω into disjoint open elements K such that $\overline{\Omega} = \cup_{K \in \mathcal{T}_h} \overline{K}$, where each $K \in \mathcal{T}_h$ is the affine image of a fixed master element $\widehat{K}$, *i.e.*, $K = F_K(\widehat{K})$, and $\widehat{K}$ is either the open unit d-simplex or the open unit hypercube in $\mathbb{R}^d$, $d = 2, 3$. For a given mesh $\mathcal{T}_h$, we define $h = \max_{K \in \mathcal{T}_h} h_K$ with $h_K = \operatorname{diam}(K)$. Notice that the mesh may contain hanging nodes. We collect all the interior (boundary, respectively) faces in the set $\mathcal{F}_h^o$ ($\mathcal{F}_h^\partial$, respectively) and set $\mathcal{F}_h = \mathcal{F}_h^o \cup \mathcal{F}_h^\partial$. In particular $\mathcal{F}_h^\partial = \mathcal{F}_h^D \cup \mathcal{F}_h^N$, where $\mathcal{F}_h^D = \mathcal{F}_h^\partial \cap \Gamma_D$ and $\mathcal{F}_h^N = \mathcal{F}_h^\partial \cap \Gamma_N$ contain respectively all Dirichlet and Neumann boundary faces. Implicit in these definitions is the assumption that $\mathcal{T}_h$ respect the decomposition of $\partial\Omega$ in the sense that any $F \in \mathcal{F}_h^\partial$ belongs to the interior of exactly one of $\mathcal{F}_h^D$ or $\mathcal{F}_h^N$. An interior face (for $d = 2$, "face" means "edge") of $\mathcal{T}_h$ is defined as the (non–empty) interior of $\partial\overline{K}^+ \cap \partial\overline{K}^-$, where K^+ and K^- are two adjacent elements of $\mathcal{T}_h$. Similarly, a boundary face of $\mathcal{T}_h$ is defined as the (non-empty) interior of $\partial\overline{K} \cap \overline{\Omega}$, where K is a boundary element of $\mathcal{T}_h$. We also assume that for all $K \in \mathcal{T}_h$ and for all $F \in \mathcal{F}_h$, $h_K \lesssim h_F$, where h_F is the diameter of $F \in \mathcal{F}_h$. This last assumption implies that the maximum number of hanging nodes on each face is uniformly bounded. Finally, we assume that a *bounded local variation* property holds (see [21]): for any pair of elements K^+ and K^- sharing a $(d-1)$–dimensional face $h_{K^-} \leq h_{K^+} \lesssim h_{K^-}$. For $s \geq 1$, we define the *broken* Sobolev spaces

$$\mathbf{H}^s(\mathcal{T}_h) = \left\{ \mathbf{v} \in \mathbf{L}^2(\Omega) \text{ such that } \mathbf{v}\big|_K \in \mathbf{H}^s(K) \quad \forall\, K \in \mathcal{T}_h \right\},$$
$$\boldsymbol{\mathcal{H}}^s(\mathcal{T}_h) = \left\{ \boldsymbol{\tau} \in \boldsymbol{\mathcal{L}}^2(\Omega) \text{ such that } \boldsymbol{\tau}\big|_K \in \boldsymbol{\mathcal{H}}^s(K) \quad \forall\, K \in \mathcal{T}_h \right\}.$$

We will also denote by $(\cdot\,,\cdot)_{\mathcal{T}_h}$ and $\langle \cdot\,, \cdot \rangle_{\mathcal{F}_h}$ the $\mathbf{L}^2(\mathcal{T}_h)$ and $\mathbf{L}^2(\mathcal{F}_h)$ inner products, respectively, and use the convention that

$$(\boldsymbol{\varphi}, \boldsymbol{\psi})_{\mathcal{T}_h} = \sum_{K \in \mathcal{T}_h} (\boldsymbol{\varphi}, \boldsymbol{\psi})_K \qquad \langle \boldsymbol{\varphi}, \boldsymbol{\psi} \rangle_{\mathcal{F}_h} = \sum_{F \in \mathcal{F}_h} (\boldsymbol{\varphi}, \boldsymbol{\psi})_F.$$

for any $\boldsymbol{\varphi}$, $\boldsymbol{\psi}$ regular enough functions. The same notation will be used for the $\boldsymbol{\mathcal{L}}^2(\mathcal{T}_h)$ and $\boldsymbol{\mathcal{L}}^2(\mathcal{F}_h)$ inner products.

3.2 Trace Operators

Let $F \in \mathcal{F}_h^o$ be an interior face shared by two elements $K^{\pm}$ of $\mathcal{T}_h$, and let $\mathbf{n}^{\pm}$ denote the normal unit vectors on F pointing outward $K^{\pm}$, respectively. For $\mathbf{v} \in \mathbf{H}^1(\mathcal{T}_h)$ and $\boldsymbol{\tau} \in \boldsymbol{\mathcal{L}}^2(\mathcal{T}_h)$ we denote by $\mathbf{v}^{\pm}$ and $\boldsymbol{\tau}^{\pm}$ the traces of $\mathbf{v}$ and $\boldsymbol{\tau}$ on F taken within the interior of $K^{\pm}$, respectively. On each $F \in \mathcal{F}_h^o$, the *weighted average* and *jump* operators are defined as

$$\begin{aligned} \{\mathbf{v}\}_\delta &= \delta \mathbf{v}^+ + (1-\delta)\mathbf{v}^-, \qquad \{\boldsymbol{\tau}\}_\delta = \delta \boldsymbol{\tau}^+ + (1-\delta)\boldsymbol{\tau}^-, \quad \delta \in [0,1], \\ [\![\mathbf{v}]\!] &= \mathbf{v}^+ \odot \mathbf{n}^+ + \mathbf{v}^- \odot \mathbf{n}^-, \quad [\![\boldsymbol{\tau}]\!] = \boldsymbol{\tau}^+ \mathbf{n}^+ + \boldsymbol{\tau}^- \mathbf{n}^-, \end{aligned} \tag{9}$$

for all $\mathbf{v} \in \mathbf{L}^2(\mathcal{T}_h)$, $\boldsymbol{\tau} \in \boldsymbol{\mathcal{L}}^2(\mathcal{T}_h)$, cf. [7]. Here $\mathbf{v} \odot \mathbf{n} = (\mathbf{v}\mathbf{n}^T + \mathbf{n}\mathbf{v}^T)/2$. Notice that with the above definitions $[\![\mathbf{v}]\!] \in \mathbb{S}$. On $F \in \mathcal{F}_h^\partial$, we set $\{\mathbf{v}\}_\delta = \mathbf{v}$, $\{\boldsymbol{\tau}\}_\delta = \boldsymbol{\tau}$, $[\![\mathbf{v}]\!] = \mathbf{v} \odot \mathbf{n}$. When $\delta = 1/2$, we drop the subindex and simply write $\{\cdot\}$. For all $\boldsymbol{\tau} \in \boldsymbol{\mathcal{L}}^2(\mathcal{T}_h)$, $\mathbf{v} \in \mathbf{H}^1(\mathcal{T}_h)$, the following identities hold

$$\sum_{K \in \mathcal{T}_h} \langle \boldsymbol{\tau}\, \mathbf{n}_K, \mathbf{v} \rangle_{\partial K} = \sum_{K \in \mathcal{T}_h} \langle \mathbf{v} \otimes \mathbf{n}_K, \boldsymbol{\tau} \rangle_{\partial K} = \langle \{\boldsymbol{\tau}\}, [\![\mathbf{v}]\!] \rangle_{\mathcal{F}_h} + \langle [\![\boldsymbol{\tau}]\!], \{\mathbf{v}\} \rangle_{\mathcal{F}_h^o}, \tag{10}$$

$$\left\langle \mathbf{v}^{\pm}, \{\boldsymbol{\tau}\}_\delta \mathbf{n}^{\pm} \right\rangle_{\mathcal{F}_h} = \left\langle \{\boldsymbol{\tau}\}_\delta, \mathbf{v}^{\pm} \odot \mathbf{n}^{\pm} \right\rangle_{\mathcal{F}_h}, \tag{11}$$

where $\mathbf{n}_K$ is the outward unit normal to ∂K. >From (11) and observing that

$$\{\boldsymbol{\tau}\}_\delta \mathbf{n}^+ = \{\boldsymbol{\tau}\}\mathbf{n}^+ + \frac{(2\delta - 1)}{2} [\![\boldsymbol{\tau}]\!] \quad \forall\, \delta \in [0,1] \quad \forall F \in \mathcal{F}_h^o, \tag{12}$$

it also easily follows

$$-\langle \{\mathbf{v}\}_{(1-\delta)} - \{\mathbf{v}\}, [\![\boldsymbol{\tau}]\!] \rangle_{\mathcal{F}_h^o} = \langle \{\boldsymbol{\tau}\}_\delta - \{\boldsymbol{\tau}\}, [\![\mathbf{v}]\!] \rangle_{\mathcal{F}_h^o}. \tag{13}$$

We finally observe that, in [4,45] the following slightly different definition of the jump operator is considered

$$[\![\![\mathbf{v}]\!]\!] = \mathbf{v}^+ \otimes \mathbf{n}^+ + \mathbf{v}^- \otimes \mathbf{n}^- \quad [\![\![\mathbf{v}]\!]\!] = \mathbf{v} \otimes \mathbf{n} \quad \forall F \in \mathcal{F}_h^\partial,$$

from which it follows that $[\![\![\mathbf{v}]\!]\!]$ is still a tensor but it is not necessarily symmetric. Nevertheless, it is easy to prove that the following identity holds

$$\langle [\![\![\mathbf{v}]\!]\!], \{\boldsymbol{\tau}\} \rangle_{\mathcal{F}_h^o} = \langle [\![\mathbf{v}]\!], \{\boldsymbol{\tau}\} \rangle_{\mathcal{F}_h^o} \quad \forall \boldsymbol{\tau} \in \boldsymbol{\mathcal{H}}^1(\mathcal{T}_h).$$

3.3 Finite Element Spaces

For $k \geq 1$ we define

$$\begin{aligned} \boldsymbol{V}_h &= \left\{ \mathbf{u} \in \mathbf{L}^2(\Omega) \ : \ \mathbf{u} \circ F_K \in [\mathcal{M}^k(\widehat{K})]^d \quad \forall\, K \in \mathcal{T}_h \right\}, \\ \boldsymbol{\Sigma}_h &= \left\{ \boldsymbol{\tau} \in \boldsymbol{\mathcal{L}}^2(\Omega) \ : \ \boldsymbol{\tau} \circ F_K \in [\mathcal{M}^k(\widehat{K})]^{d \times d} \quad \forall\, K \in \mathcal{T}_h \right\}, \end{aligned}$$

where $\mathcal{M}^k(\widehat{K})$ is either the space $\mathbb{P}^k(\widehat{K})$ of polynomials of degree at most k on $\widehat{K}$, if $\widehat{K}$ is the reference d-simplex, or the space $\mathbb{Q}^k(\widehat{K})$ of tensor–product polynomials on $\widehat{K}$ of degree k in each coordinate direction, if $\widehat{K}$ is the unit reference hypercube in $\mathbb{R}^d$.

3.4 Technical Tools

For any $\mathbf{v} \in \mathbf{H}^1(K)$, Agmon' inequality reads

$$\|\mathbf{v}\|_{0,F}^2 \lesssim h_K^{-1} \|\mathbf{v}\|_{0,K}^2 + h_K |\mathbf{v}|_{1,K}^2 \quad \forall\, F \in \mathcal{F}_h,\, F \subset \partial K, \tag{14}$$

where the hidden constant is independent of the mesh size but depends on the polynomial degree when applied to discrete functions. For discrete functions, we will also frequently use the following inequality:

$$h\|\mathbf{v}\|_{0,F}^2 \lesssim \|\mathbf{v}\|_{0,K}^2 \quad \forall\, F \in \mathcal{F}_h,\, F \subset \partial K. \tag{15}$$

The L^p-version of the above inequality, which holds for discrete functions $\mathbf{v} \in \boldsymbol{W}^{1,p}(K)$, reads

$$h^{1/p}\|\mathbf{v}\|_{L^p(F)} \lesssim \|\mathbf{v}\|_{L^p(K)} \quad 1 \le p \le \infty\,, \tag{16}$$

cf. [14]. Let ω be either an element, an edge or a face of the decomposition $\mathcal{T}_h$, and let $\mathbf{v}$ be a polynomial of degree $k \ge 1$ defined on ω, then

$$\|\mathbf{v}\|_{L^p(\omega)} \lesssim \mathrm{meas}(\omega)^{\left(\frac{1}{p}-\frac{1}{q}\right)}\|\mathbf{v}\|_{L^q(\omega)} \quad 1 \le p, q \le \infty\,. \tag{17}$$

Finally, for any $K \in \mathcal{T}_h$ the inverse inequality can be written as

$$|\mathbf{v}|_{m,K} \lesssim h_K^{s-m}|\mathbf{v}|_{s,K} \quad \forall\, \mathbf{v} \in \boldsymbol{V}_h, \quad s \le m. \tag{18}$$

The hidden constants in (15),(16),(17) and (18) are independent of the mesh size but depend on the polynomial degree.

4 Discontinuous Galerkin Approximations

In this section, we introduce the family of semidiscrete DG approximations to (6a)–(6b) that we consider in this work. The derivation of the methods follows closely [6], with a slight difference though when introducing the schemes for the *displacement* formulation. We start by considering a general variational formulation for DG methods: given $(\mathbf{u}^h(0), \mathbf{u}_t^h(0))$ two suitable approximations to the initial data that will be defined later on, find $(\mathbf{u}^h, \boldsymbol{\sigma}^h) \in C^2((0,T];\boldsymbol{V}_h) \times C^0((0,T];\boldsymbol{\Sigma}_h)$ such that for all $\mathbf{v} \in \boldsymbol{V}_h$, $\boldsymbol{\tau} \in \boldsymbol{\Sigma}_h$

$$\begin{aligned}
&\left(\rho\mathbf{u}_{tt}^h, \mathbf{v}\right)_{\mathcal{T}_h} + \left(\boldsymbol{\sigma}^h, \boldsymbol{\varepsilon}(\mathbf{v})\right)_{\mathcal{T}_h} - \langle\{\widehat{\boldsymbol{\sigma}}\}, [\![\mathbf{v}]\!]\rangle_{\mathcal{F}_h} - \langle[\![\widehat{\boldsymbol{\sigma}}]\!], \{\mathbf{v}\}\rangle_{\mathcal{F}_h^o} = (\mathbf{f}, \mathbf{v})_{\mathcal{T}_h},\\
&\left(\mathcal{A}\boldsymbol{\sigma}^h, \boldsymbol{\tau}\right)_{\mathcal{T}_h} - \left(\boldsymbol{\varepsilon}(\mathbf{u}^h), \boldsymbol{\tau}\right)_{\mathcal{T}_h} - \left\langle\{\widehat{\mathbf{u}} - \mathbf{u}^h\}, [\![\boldsymbol{\tau}]\!]\right\rangle_{\mathcal{F}_h^o} - \left\langle[\![\widehat{\mathbf{u}} - \mathbf{u}^h]\!], \{\boldsymbol{\tau}\}\right\rangle_{\mathcal{F}_h} = 0,
\end{aligned}$$

where

$$(\widehat{\mathbf{u}}, \widehat{\boldsymbol{\sigma}}) = \left(\widehat{\mathbf{u}}(\mathbf{u}^h, \boldsymbol{\sigma}^h), \widehat{\boldsymbol{\sigma}}(\mathbf{u}^h, \boldsymbol{\sigma}^h)\right) : \left(\mathbf{H}^1(\mathcal{T}_h) \times \boldsymbol{\mathcal{H}}^1(\mathcal{T}_h)\right)^2 \longrightarrow \left(\mathbf{L}^2(\mathcal{F}_h), \boldsymbol{\mathcal{L}}^2(\mathcal{F}_h)\right),$$

are the numerical fluxes that will be properly chosen and identify the corresponding DG method. On boundary faces $F \in \mathcal{F}_h^\partial$ we always define the numerical fluxes according to the boundary conditions:

$$\begin{aligned}
&\widehat{\mathbf{u}} = \mathbf{0} && \text{on } F \in \mathcal{F}_h^D, && \widehat{\mathbf{u}} = \mathbf{u}^h - \mathbf{c}_{22}(\boldsymbol{\sigma}^h\mathbf{n} - \mathbf{g}) && \text{on } F \in \mathcal{F}_h^N,\\
&\widehat{\boldsymbol{\sigma}}\,\mathbf{n} = \boldsymbol{\sigma}^h\mathbf{n} - \mathbf{c}_{11}\mathbf{u}^h && \text{on } F \in \mathcal{F}_h^D, && \widehat{\boldsymbol{\sigma}}\,\mathbf{n} = \mathbf{g} && \text{on } F \in \mathcal{F}_h^N.
\end{aligned}$$

Here, $\mathbf{c}_{11}$ and $\mathbf{c}_{22}$ are functions (possibly equal to zero) that we will choose later on. Then, the DG formulation becomes: Find $(\mathbf{u}^h, \boldsymbol{\sigma}^h) \in C^2((0,T];\boldsymbol{V}_h) \times C^0((0,T];\boldsymbol{\Sigma}_h)$ such that

for all $\mathbf{v} \in \boldsymbol{V}_h$, $\boldsymbol{\tau} \in \boldsymbol{\Sigma}_h$ it holds

$$\left(\rho \mathbf{u}_{tt}^h, \mathbf{v}\right)_{\mathcal{T}_h} + \left(\boldsymbol{\sigma}^h, \boldsymbol{\varepsilon}(\mathbf{v})\right)_{\mathcal{T}_h} - \langle\{\widehat{\boldsymbol{\sigma}}\}, [\![\mathbf{v}]\!]\rangle_{\mathcal{F}_h^o} - \langle[\![\widehat{\boldsymbol{\sigma}}]\!], \{\mathbf{v}\}\rangle_{\mathcal{F}_h^o} + \langle \mathbf{c}_{11}\mathbf{u}^h, \mathbf{v}\rangle_{\mathcal{F}_h^D} - \langle \boldsymbol{\sigma}^h\mathbf{n}, \mathbf{v}\rangle_{\mathcal{F}_h^D} = (\mathbf{f}, \mathbf{v})_{\mathcal{T}_h} + \langle \mathbf{g}, \mathbf{v}\rangle_{\mathcal{F}_h^N}, \tag{19a}$$

$$\left(\mathcal{A}\boldsymbol{\sigma}^h - \boldsymbol{\varepsilon}(\mathbf{u}^h), \boldsymbol{\tau}\right)_{\mathcal{T}_h} - \langle\{\widehat{\mathbf{u}} - \mathbf{u}^h\}, [\![\boldsymbol{\tau}]\!]\rangle_{\mathcal{F}_h^o} - \langle[\![\widehat{\mathbf{u}} - \mathbf{u}^h]\!], \{\boldsymbol{\tau}\}\rangle_{\mathcal{F}_h^o} + \langle[\![\mathbf{u}^h]\!], \{\boldsymbol{\tau}\}\rangle_{\mathcal{F}_h^D} + \langle \mathbf{c}_{22}(\boldsymbol{\sigma}^h\mathbf{n} - \mathbf{g}), \boldsymbol{\tau}\,\mathbf{n}\rangle_{\mathcal{F}_h^N} = 0. \tag{19b}$$

We present now several methods for approximating the *displacement-stress* formulation, by selecting different choices of the numerical fluxes in (19). We restrict our attention to methods for which the numerical fluxes $\widehat{\mathbf{u}}$ and $\widehat{\boldsymbol{\sigma}}$ are singled valued, and so $[\![\widehat{\mathbf{u}}]\!] = \mathbf{0}$ and $[\![\widehat{\boldsymbol{\sigma}}]\!] = \mathbf{0}$ on internal faces.

Now, in analogy with the method introduced in [11] for second order elliptic problems, the full DG (FDG) approximation is characterized by the choices

$$\widehat{\mathbf{u}} = \{\mathbf{u}^h\}_{1-\delta} - \mathbf{c}_{22}[\![\boldsymbol{\sigma}^h]\!], \quad \widehat{\boldsymbol{\sigma}} = \{\boldsymbol{\sigma}^h\}_{\delta} - \mathbf{c}_{11}[\![\mathbf{u}^h]\!], \quad F \in \mathcal{F}_h^o, \tag{20}$$

where

$$\mathbf{c}_{11} = c_1 h_F^{-1} k^2 \{\mathcal{D}\} \quad \mathbf{c}_{22} = c_2 h_F k^{-2} \{\mathcal{D}\}^{-1} \quad F \in \mathcal{F}_h^o. \tag{21}$$

Here $c_1, c_2 \geq 0$ are constants (sometimes required to be strictly positive). On boundary faces, $\mathbf{c}_{11}$ and $\mathbf{c}_{22}$ are defined accordingly. Substituting (20) into (19), we get: Find $(\mathbf{u}^h, \boldsymbol{\sigma}^h) \in C^2((0,T]; \boldsymbol{V}_h) \times C^0((0,T]; \boldsymbol{\Sigma}_h)$ such that for all $\mathbf{v} \in \boldsymbol{V}_h$ and $\boldsymbol{\tau} \in \boldsymbol{\Sigma}_h$

$$\begin{aligned}
&\left(\rho \mathbf{u}_{tt}^h, \mathbf{v}\right)_{\mathcal{T}_h} + \left(\boldsymbol{\sigma}^h, \boldsymbol{\varepsilon}(\mathbf{v})\right)_{\mathcal{T}_h} - \langle\{\boldsymbol{\sigma}^h\}_{\delta} - \mathbf{c}_{11}[\![\mathbf{u}^h]\!], [\![\mathbf{v}]\!]\rangle_{\mathcal{F}_h^o} \\
&\quad + \langle \mathbf{c}_{11}\mathbf{u}^h, \mathbf{v}\rangle_{\mathcal{F}_h^D} - \langle \boldsymbol{\sigma}^h\mathbf{n}, \mathbf{v}\rangle_{\mathcal{F}_h^D} = (\mathbf{f}, \mathbf{v})_{\mathcal{T}_h} + \langle \mathbf{g}, \mathbf{v}\rangle_{\mathcal{F}_h^N}, \\
&\left(\mathcal{A}\boldsymbol{\sigma}^h - \boldsymbol{\varepsilon}(\mathbf{u}^h), \boldsymbol{\tau}\right)_{\mathcal{T}_h} - \langle\{\mathbf{u}^h\}_{(1-\delta)} - \{\mathbf{u}^h\}, [\![\boldsymbol{\tau}]\!]\rangle_{\mathcal{F}_h^o} + \langle \mathbf{c}_{22}[\![\boldsymbol{\sigma}^h]\!], [\![\boldsymbol{\tau}]\!]\rangle_{\mathcal{F}_h^o} \\
&\quad + \langle[\![\mathbf{u}^h]\!], \{\boldsymbol{\tau}\}\rangle_{\mathcal{F}_h^o \cup \mathcal{F}_h^D} + \langle \mathbf{c}_{22}(\boldsymbol{\sigma}^h\mathbf{n} - \mathbf{g}), \boldsymbol{\tau}\,\mathbf{n}\rangle_{\mathcal{F}_h^N} = 0.
\end{aligned} \tag{22}$$

Special cases are the *local discontinuous Galerkin* (LDG) method and the *alternating choice of fluxes* (ALT) methods. The former is characterized by setting $\mathbf{c}_{22} = \mathbf{0}$, whereas the latter by $\mathbf{c}_{22} = \mathbf{c}_{11} = \mathbf{0}$ and $\delta = 1$ or $\delta = 0$. For $\delta = 1$ the numerical fluxes become

$$\widehat{\mathbf{u}} = (\mathbf{u}^h)^-, \quad \widehat{\boldsymbol{\sigma}} = (\boldsymbol{\sigma}^h)^+. \tag{23}$$

This choice has been frequently used to design DG approximation for time dependent problems with high order derivatives [13,54]. To our knowledge, the ALT method has never been considered for the elastodynamics problem. In the next section, we will show that stability for the ALT method can be guaranteed only in the case of Dirichlet-type boundary conditions (or periodic boundary conditions, generally used in [13,54], but not realistic in the present context).

We now consider DG methods in *displacement* formulation. To obtain the variational formulation starting from (19), the numerical flux $\widehat{\boldsymbol{\sigma}}$ is defined as a function of $\mathbf{u}^h$. More precisely, for $\delta \in [0,1]$, we specify $\widehat{\boldsymbol{\sigma}}$ as follows

$$\widehat{\boldsymbol{\sigma}} = \begin{cases} \{\mathcal{D}\boldsymbol{\varepsilon}(\mathbf{u}^h)\}_{\delta} - \mathbf{S}_F[\![\mathbf{u}^h]\!] & F \in \mathcal{F}_h^o, \\ \mathcal{D}\boldsymbol{\varepsilon}(\mathbf{u}^h) - \mathbf{S}_F\mathbf{u}^h\mathbf{n} & F \in \mathcal{F}_h^D, \end{cases} \tag{24}$$

where

$$\mathbf{S}_F = \mathbf{c}_{00} h_F^{-1} k^2 \{\mathcal{D}\} \quad \forall\, F \in \mathcal{F}_h^o \cup \mathcal{F}_h^D, \tag{25}$$

and $\mathbf{c}_{00}$ is a strictly positive constant that has to be chosen sufficiently large, see below. To be consistent, we have replaced the parameter $\mathbf{c}_{11}$ by $\mathbf{S}_F$, which plays the same role and scales in the same way (see below for its precise definition), but, differently from $\mathbf{c}_{11}$, will undergo to a technical restriction. The definition of the numerical fluxes on boundary faces has to be modified taking into account that $\boldsymbol{\sigma}^h \mathbf{n} = \mathcal{D}\boldsymbol{\varepsilon}(\mathbf{u}^h)\mathbf{n}$ on $\mathcal{F}_h^\partial$ (and $\mathbf{c}_{22} \equiv \mathbf{0}$ now). Hence, we have:

$$\begin{aligned} \widehat{\mathbf{u}} &= \mathbf{0} && \text{on } F \in \mathcal{F}_h^D, \qquad \widehat{\mathbf{u}} = \mathbf{u}^h \quad \text{on } F \in \mathcal{F}_h^N, \\ \widehat{\boldsymbol{\sigma}}\,\mathbf{n} &= \mathcal{D}\boldsymbol{\varepsilon}(\mathbf{u}^h)\mathbf{n} - \mathbf{S}_F \mathbf{u}^h && \text{on } F \in \mathcal{F}_h^D, \quad \widehat{\boldsymbol{\sigma}}\,\mathbf{n} = \mathbf{g} \quad \text{on } F \in \mathcal{F}_h^N. \end{aligned}$$

Assuming now that the finite element spaces $(\boldsymbol{V}_h, \boldsymbol{\Sigma}_h)$ are such that $\boldsymbol{\varepsilon}(\boldsymbol{V}_h) \subseteq \boldsymbol{\Sigma}_h$ and setting $\boldsymbol{\tau} = \mathcal{D}\boldsymbol{\varepsilon}(\mathbf{v}) \in \boldsymbol{\Sigma}_h$ in (19b) we find for all $\mathbf{v} \in \boldsymbol{V}_h$:

$$\begin{aligned} \Big(\mathcal{A}\boldsymbol{\sigma}^h, \mathcal{D}\boldsymbol{\varepsilon}(\mathbf{v})\Big)_{\mathcal{T}_h} = \Big(\boldsymbol{\varepsilon}(\mathbf{u}^h), \mathcal{D}\boldsymbol{\varepsilon}(\mathbf{v})\Big)_{\mathcal{T}_h} &+ \langle \{\widehat{\mathbf{u}} - \mathbf{u}^h\}, [\![\mathcal{D}\boldsymbol{\varepsilon}(\mathbf{v})]\!] \rangle_{\mathcal{F}_h^o} \\ &+ \langle [\![\widehat{\mathbf{u}} - \mathbf{u}^h]\!], \{\mathcal{D}\boldsymbol{\varepsilon}(\mathbf{v})\} \rangle_{\mathcal{F}_h^o \cup \mathcal{F}_h^D}\,. \end{aligned}$$

Since $\mathcal{A}$ is symmetric and positive definite it holds

$$\Big(\mathcal{A}\boldsymbol{\sigma}^h, \mathcal{D}\boldsymbol{\varepsilon}(\mathbf{v})\Big)_{\mathcal{T}_h} = \Big(\boldsymbol{\sigma}^h, \mathcal{A}^\top \mathcal{D}\boldsymbol{\varepsilon}(\mathbf{v})\Big)_{\mathcal{T}_h} = (\boldsymbol{\sigma}^h, \boldsymbol{\varepsilon}(\mathbf{v}))_{\mathcal{T}_h} \quad \forall\, \mathbf{v} \in \boldsymbol{V}_h,$$

and so,

$$\begin{aligned} (\boldsymbol{\sigma}^h, \boldsymbol{\varepsilon}(\mathbf{v}))_{\mathcal{T}_h} = (\boldsymbol{\varepsilon}(\mathbf{u}^h), \mathcal{D}\boldsymbol{\varepsilon}(\mathbf{v}))_{\mathcal{T}_h} &+ \langle \{\widehat{\mathbf{u}} - \mathbf{u}^h\}, [\![\mathcal{D}\boldsymbol{\varepsilon}(\mathbf{v})]\!] \rangle_{\mathcal{F}_h^o} \\ &+ \langle [\![\widehat{\mathbf{u}} - \mathbf{u}^h]\!], \{\mathcal{D}\boldsymbol{\varepsilon}(\mathbf{v})\} \rangle_{\mathcal{F}_h^o \cup \mathcal{F}_h^D}. \end{aligned}$$

Combining now the above equation together with (19a) and the definition of numerical flux $\widehat{\boldsymbol{\sigma}}$ given in (24), we finally get the following formulation: Find $\mathbf{u}^h \in C^2((0,T]; \boldsymbol{V}_h)$ such that for all $\mathbf{v} \in \boldsymbol{V}_h$

$$\begin{aligned} &\Big(\rho \mathbf{u}_{tt}^h, \mathbf{v}\Big)_{\mathcal{T}_h} + \Big(\boldsymbol{\varepsilon}(\mathbf{u}^h), \mathcal{D}\boldsymbol{\varepsilon}(\mathbf{v})\Big)_{\mathcal{T}_h} + \langle \{\widehat{\mathbf{u}} - \mathbf{u}^h\}, [\![\mathcal{D}\boldsymbol{\varepsilon}(\mathbf{v})]\!] \rangle_{\mathcal{F}_h^o} + \langle [\![\widehat{\mathbf{u}} - \mathbf{u}^h]\!], \{\mathcal{D}\boldsymbol{\varepsilon}(\mathbf{v})\} \rangle_{\mathcal{F}_h^o \cup \mathcal{F}_h^D} \\ &- \langle \{\mathcal{D}\boldsymbol{\varepsilon}(\mathbf{u}^h)\}_\delta, [\![\mathbf{v}]\!] \rangle_{\mathcal{F}_h^o \cup \mathcal{F}_h^D} + \langle \mathbf{S}_F [\![\mathbf{u}^h]\!], [\![\mathbf{v}]\!] \rangle_{\mathcal{F}_h^o \cup \mathcal{F}_h^D} = (\mathbf{f}, \mathbf{v})_{\mathcal{T}_h} + \langle \mathbf{g}, \mathbf{v} \rangle_{\mathcal{F}_h^N}, \end{aligned}$$

which corresponds to the family of classical Interior Penalty (IP) methods. Following [49], to obtain the weighted Symmetric Interior Penalty method (SIP(δ)) we define

$$\widehat{\mathbf{u}} = \{\mathbf{u}^h\}_{1-\delta} \quad \forall \delta \in [0,1].$$

For $\delta = 1/2$, $\widehat{\mathbf{u}} = \{\mathbf{u}^h\}$, we get the classical Symmetric Interior Penalty (SIP) method [5].

The weak formulation reads: find $\mathbf{u}^h \in C^2([0,T]; \boldsymbol{V}_h)$ such that

$$\Big(\rho \mathbf{u}_{tt}^h, \mathbf{v}\Big)_{\mathcal{T}_h} + a(\mathbf{u}^h, \mathbf{v}) = (\mathbf{f}, \mathbf{v})_{\mathcal{T}_h} + \langle \mathbf{g}, \mathbf{v} \rangle_{\mathcal{F}_h^N} \quad \forall\, \mathbf{v} \in \boldsymbol{V}_h, \tag{26}$$

where $a(\cdot,\cdot) : \boldsymbol{V}_h \times \boldsymbol{V}_h \longrightarrow \mathbb{R}$ is given by

$$\begin{aligned} a(\mathbf{w}, \mathbf{v}) = (\boldsymbol{\varepsilon}(\mathbf{w}), \mathcal{D}\boldsymbol{\varepsilon}(\mathbf{v}))_{\mathcal{T}_h} &- \langle \{\mathcal{D}\boldsymbol{\varepsilon}(\mathbf{w})\}_\delta, [\![\mathbf{v}]\!] \rangle_{\mathcal{F}_h^o \cup \mathcal{F}_h^D} - \langle [\![\mathbf{w}]\!], \{\mathcal{D}\boldsymbol{\varepsilon}(\mathbf{v})\}_\delta \rangle_{\mathcal{F}_h^o \cup \mathcal{F}_h^D} \\ &+ \langle \mathbf{S}_F [\![\mathbf{w}]\!], [\![\mathbf{v}]\!] \rangle_{\mathcal{F}_h^o \cup \mathcal{F}_h^D}. \end{aligned} \tag{27}$$

5 Stability

We now prove stability in the natural energy norm induced by the DG methods described in Sect. 4. For the DG methods in *displacement-stress* formulation (22) we define the energy norm

$$\left\|(\mathbf{u}^h(t),\boldsymbol{\sigma}^h(t))\right\|^2_{\mathcal{E},\mathrm{MDG}} = \left\|\rho^{1/2}\mathbf{u}^h_t(t)\right\|^2_{0,\mathcal{T}_h} + \left\|\mathcal{A}^{1/2}\boldsymbol{\sigma}^h(t)\right\|^2_{0,\mathcal{T}_h} + \left\|\mathbf{c}_{11}^{1/2}[\![\mathbf{u}^h(t)]\!]\right\|^2_{0,\mathcal{F}_h^o\cup\mathcal{F}_h^D} + \left\|\mathbf{c}_{22}^{1/2}[\![\boldsymbol{\sigma}^h(t)]\!]\right\|^2_{0,\mathcal{F}_h^o\cup\mathcal{F}_h^N} \tag{28}$$

for any $(\mathbf{u}^h,\boldsymbol{\sigma}^h)\in C^2([0,T];\boldsymbol{V}_h)\times C^0([0,T];\boldsymbol{\Sigma}_h)$ and any $t\in[0,T]$. For the LDG and ALT methods, one needs to set above $\mathbf{c}_{22}=\mathbf{0}$ and $\mathbf{c}_{11}=\mathbf{c}_{22}=\mathbf{0}$, respectively. For the DG methods in *displacement* formulation, the energy norm is defined for all $\mathbf{u}^h\in C^2([0,T];\boldsymbol{V}_h)$ as follows

$$\left\|\mathbf{u}^h(t)\right\|^2_{\mathcal{E},\mathrm{IP}} = \|\rho^{1/2}\mathbf{u}^h_t\|^2_{0,\mathcal{T}_h} + \|\mathcal{D}^{1/2}\boldsymbol{\varepsilon}(\mathbf{u}^h(t))\|^2_{0,\mathcal{T}_h} + \|\mathbf{S}_F^{1/2}[\![\mathbf{u}^h(t)]\!]\|^2_{0,\mathcal{F}_h^o\cup\mathcal{F}_h^D} \tag{29}$$

for all $t\in[0,T]$. For further use, we also define the norm

$$\left\|\mathbf{u}^h(t)\right\|^2_{a} = \|\mathcal{D}^{1/2}\boldsymbol{\varepsilon}(\mathbf{u}^h(t))\|^2_{0,\mathcal{T}_h} + \left\|\{\mathcal{D}\}^{1/2}h_F^{-1/2}[\![\mathbf{u}^h(t)]\!]\right\|^2_{0,\mathcal{F}_h^o\cup\mathcal{F}_h^D}. \tag{30}$$

Moreover, with a small abuse of notation, for $t=0$ we write

$$\left\|(\mathbf{u}^h_0,\boldsymbol{\sigma}^h_0)\right\|^2_{\mathcal{E},\mathrm{MDG}} = \left\|\rho^{1/2}\mathbf{u}^h_1\right\|^2_{0,\mathcal{T}_h} + \left\|\mathcal{A}^{1/2}\boldsymbol{\sigma}^h_0\right\|^2_{0,\mathcal{T}_h} + \left\|\mathbf{c}_{11}^{1/2}[\![\mathbf{u}^h_0]\!]\right\|^2_{0,\mathcal{F}_h^o\cup\mathcal{F}_h^D} + \left\|\mathbf{c}_{22}^{1/2}[\![\boldsymbol{\sigma}^h_0]\!]\right\|^2_{0,\mathcal{F}_h^o\cup\mathcal{F}_h^N},$$

$$\left\|\mathbf{u}^h_0\right\|^2_{\mathcal{E},\mathrm{IP}} = \left\|\rho^{1/2}\mathbf{u}^h_1\right\|^2_{0,\mathcal{T}_h} + \left\|\mathcal{D}^{1/2}\boldsymbol{\varepsilon}(\mathbf{u}^h_0)\right\|^2_{0,\mathcal{T}_h} + \left\|\mathbf{S}_F^{1/2}[\![\mathbf{u}^h_0]\!]\right\|^2_{0,\mathcal{F}_h^o\cup\mathcal{F}_h^D},$$

$$\left\|\mathbf{u}^h_0\right\|^2_{a} = \left\|\mathcal{D}^{1/2}\boldsymbol{\varepsilon}(\mathbf{u}^h_0)\right\|^2_{0,\mathcal{T}_h} + \left\|\{\mathcal{D}\}^{1/2}h_F^{-1/2}[\![\mathbf{u}^h_0]\!]\right\|^2_{0,\mathcal{F}_h^o\cup\mathcal{F}_h^D},$$

where $(\mathbf{u}^h_0,\mathbf{u}^h_1)$ and $\boldsymbol{\sigma}^h_0$ are some projections of $(\mathbf{u}_0,\mathbf{u}_1)$ and $\boldsymbol{\sigma}(0,x)$ onto the finite element spaces $\boldsymbol{V}_h$ and $\boldsymbol{\Sigma}_h$, respectively.

The main results of this section are contained in the following two propositions.

Proposition 1 *Let $(\mathbf{u}^h,\boldsymbol{\sigma}^h)\in C^2((0,T];\boldsymbol{V}_h)\times C^0((0,T];\boldsymbol{\Sigma}_h)$ be the approximate solution obtained with any of the DG methods for the displacement-stress formulation introduced in Sect. 4.*

(i) *In the absence of external forces, i.e., $\mathbf{f}=\mathbf{g}=\mathbf{0}$, FDG, LDG and ALT methods are fully conservative:*

$$\left\|(\mathbf{u}^h(t),\boldsymbol{\sigma}^h(t))\right\|_{\mathcal{E},MDG} = \left\|(\mathbf{u}^h_0,\boldsymbol{\sigma}^h_0)\right\|_{\mathcal{E},MDG}, \qquad 0<t\le T.$$

(ii) *If $\mathbf{f}\in L^2((0,T];\mathbf{L}^2(\Omega))$ and $\partial\Omega=\Gamma_D$, the FDG, LDG and ALT methods satisfy the following* a priori *discrete energy estimate:*

$$\left\|(\mathbf{u}^h(t),\boldsymbol{\sigma}^h(t))\right\|_{\mathcal{E},MDG} \lesssim \left\|(\mathbf{u}^h_0,\boldsymbol{\sigma}^h_0)\right\|_{\mathcal{E},MDG} + \int_0^t \rho_*^{-1/2}\|\mathbf{f}(\tau)\|_{0,\Omega}d\tau \quad 0<t\le T.$$

(iii) *If* $\mathbf{f} \in L^2((0,T];\mathbf{L}^2(\Omega))$ *and* $\mathbf{g} \in C^1((0,T];\mathbf{H}^1(\Gamma_N))$, *the FDG and LDG methods satisfy the following* a priori *discrete energy estimate: for all* $0 < t \leq T$

$$\left\|(\mathbf{u}^h(t),\boldsymbol{\sigma}^h(t))\right\|_{\mathcal{E},MDG} \lesssim \sqrt{\mathcal{G}_{MDG}} + \int_0^t \left(\rho_*^{-1/2}\|\mathbf{f}(\tau)\|_{0,\Omega} + \mathrm{D}_*^{-1/2}\,\|\mathbf{g}_\tau(\tau)\|_{1,\Gamma_N}\right) d\tau,$$

where $\mathbf{g}_\tau$ *denotes the time derivative of* $\mathbf{g}$ *and*

$$\mathcal{G}_{MDG} = \left\|(\mathbf{u}_0^h,\boldsymbol{\sigma}_0^h)\right\|^2_{\mathcal{E},MDG} + \mathrm{D}_*^{-1}\left(\|\mathbf{g}_0\|^2_{1,\Gamma_N} + \sup_{0<t\leq T}\|\mathbf{g}(t)\|^2_{1,\Gamma_N}\right) + \int_0^t \mathrm{D}_*^{-1}\,\|\mathbf{g}_\tau\|_{1,\Gamma_N}\,\|\mathbf{g}\|_{1/2,\Gamma_N}\,d\tau\ .$$

For the IP(δ) method, the stability result reads as follows.

Proposition 2 *Let the penalty parameter* $\mathbf{c}_{00}$ *in* (25) *be large enough and let* $\mathbf{u}^h \in C^2((0,T];V_h)$ *be the corresponding approximate solution obtained with the SIP(δ) method introduced in Sect. 4 with such* $\mathbf{c}_{00}$.

(i) *In the absence of external forces, i.e.,* $\mathbf{f} = \mathbf{g} = \mathbf{0}$,

$$\left\|\mathbf{u}^h(t)\right\|_{\mathcal{E},IP} \lesssim \left\|\mathbf{u}_0^h\right\|_{\mathcal{E},IP}, \quad 0 < t \leq T;$$

(ii) *If* $\mathbf{f} \in L^2((0,T];\mathbf{L}^2(\Omega))$ *and* $\mathbf{g} \in C^1((0,T];\mathbf{H}^1(\Gamma_N))$, *then*

$$\left\|\mathbf{u}^h(t)\right\|^2_{\mathcal{E},IP} \lesssim \sqrt{\mathcal{G}_{IP}} + \int_0^t \left(\rho_*^{-1}\|\mathbf{f}(\tau)\|_{0,\Omega} + \|\mathbf{g}_\tau(\tau)\|_{1,\Gamma_N}\right) d\tau \quad 0 < t \leq T,$$

where

$$\mathcal{G}_{IP} = \left\|\mathbf{u}_0^h\right\|^2_{\mathcal{E},IP} + \mathrm{D}_*^{-1}\sup_{0<t\leq T}\|\mathbf{g}(t)\|^2_{1,\Gamma_N} + \mathrm{D}_*^{-1}\|\mathbf{g}_0\|^2_{1,\Gamma_N}.$$

In the case of boundary conditions of mixed type, Propositions 1 and 2 would require the traction boundary data $\mathbf{g}$ to be more regular that what is required by the continuous problem. Whether this is a technical restriction due to an artifact of our proof or it is really necessary to ensure stability of the methods is an open issue. This restriction comes into play from the proof of Lemma 1.

We next state two auxiliary results. Their proofs are given in "Appendix".

Lemma 1 *Let* $\mathbf{f} \in L^2((0,T];\mathbf{L}^2(\Omega))$ *and* $\mathbf{g} \in C^1((0,T];\mathbf{H}^{1/2}(\Gamma_N))$. *Let* $(\mathbf{u}^h,\boldsymbol{\sigma}^h) \in C^2((0,T];V_h)\times C^0((0,T];\boldsymbol{\Sigma}_h)$ *be the DG approximation to the solution* $(\mathbf{u},\boldsymbol{\sigma})$ *of problem* (6a)–(6b) *obtained with any of the DG methods introduced in Sect. 4. Then, the following bounds hold:*

$$\left|\int_0^t (\mathbf{f}(\tau),\mathbf{u}_\tau^h(\tau))_{\mathcal{T}_h}\,d\tau\right| \leq \int_0^t \rho_*^{-1/2}\|\mathbf{f}(\tau)\|_{0,\Omega}\|\rho^{1/2}\mathbf{u}_\tau^h(\tau)\|_{0,\mathcal{T}_h}\,d\tau\ , \tag{31}$$

$$\left|\int_0^t \langle \mathbf{c}_{22}\mathbf{g}_\tau(\tau),\boldsymbol{\sigma}^h(\tau)\,\mathbf{n}\rangle_{\mathcal{F}_h^N}\,d\tau\right| \lesssim \int_0^t \mathrm{D}_*^{-1/2}\|\mathbf{g}_\tau(\tau)\|_{1/2,\Gamma_N}\|\mathbf{c}_{22}^{1/2}\boldsymbol{\sigma}^h(\tau)\mathbf{n}\|_{0,\mathcal{F}_h^N}d\tau, \tag{32}$$

where $\mathbf{c}_{22}$ *is defined as in* (21) *and* D_*, ρ_* *are given in* (5) *and* (2), *respectively. Furthermore, if* $\mathbf{g} \in C^1((0,T];\mathbf{H}^1(\Gamma_N))$, *then for any* $\epsilon > 0$, *it holds*

$$\left|\int_0^t \langle \mathbf{g}(\tau),\mathbf{u}_\tau^h(\tau)\rangle_{0,\mathcal{F}_h^N}\,d\tau\right| \lesssim \epsilon\left\|\mathbf{u}^h(t)\right\|_a^2 + \mathrm{D}_*^{-1/2}\left\|\mathbf{u}_0^h\right\|_a\|\mathbf{g}_0\|_{1,\Gamma_N} + \frac{\mathrm{D}_*^{-1}}{\epsilon}\|\mathbf{g}(t)\|^2_{1,\Gamma_N} + \int_0^t \mathrm{D}_*^{-1/2}\|\mathbf{g}_\tau(\tau)\|_{1,\Gamma_N}\left\|\mathbf{u}^h(\tau)\right\|_a\,d\tau. \tag{33}$$

The following result provides a bound of the norm of the symmetric discrete gradient in terms of the discrete stress tensor, and will be required in the proof of Proposition 1.

Lemma 2 *Let* $\mathbf{f} \in L^2((0,T];\mathbf{L}^2(\Omega))$ *and* $\mathbf{g} \in C^1((0,T];\mathbf{H}^{1/2}(\Gamma_N))$. *Let* $(\mathbf{u}^h,\boldsymbol{\sigma}^h) \in C^2((0,T];\boldsymbol{V}_h)\times C^0((0,T];\boldsymbol{\Sigma}_h)$ *be the approximate solution to* (6a)–(6b) *obtained with any of the DG methods for displacement-stress formulation introduced in Sect. 4. Then, the following bound holds:*

$$\|\mathcal{D}^{1/2}\boldsymbol{\varepsilon}(\mathbf{u}^h)\|_{0,\mathcal{T}_h} \lesssim \|\mathcal{A}^{1/2}\boldsymbol{\sigma}^h\|_{0,\mathcal{T}_h} + \|\mathbf{c}_{11}^{1/2}[\![\mathbf{u}^h]\!]\|_{0,\mathcal{F}_h^o} + \|\mathbf{c}_{22}^{1/2}[\![\boldsymbol{\sigma}^h]\!]\|_{0,\mathcal{F}_h^N} + \mathrm{D}_*^{-1}\|\mathbf{g}\|^2_{1/2,\Gamma_N}, \tag{34}$$

where D_* *is given in* (5). *For the LDG method the last two terms on the right hand side are not present in the bound.*

Proof (Proof of Proposition 1) To simplify the notation we drop the explicit dependence on t.

Step 1. We take $\mathbf{v} = \mathbf{u}_t^h \in \boldsymbol{V}_h$ as test function in the first equation of (19a) and use $[\![\widehat{\boldsymbol{\sigma}}]\!] = \mathbf{0}$ to obtain

$$\left(\rho\mathbf{u}_{tt}^h, \mathbf{u}_t^h\right)_{\mathcal{T}_h} + \left(\boldsymbol{\sigma}^h, \boldsymbol{\varepsilon}(\mathbf{u}_t^h)\right)_{\mathcal{T}_h} - \langle\{\widehat{\boldsymbol{\sigma}}\}, [\![\mathbf{u}_t^h]\!]\rangle_{\mathcal{F}_h^o\cup\mathcal{F}_h^D} = (\mathbf{f},\mathbf{u}_t^h)_{\mathcal{T}_h} + \langle\mathbf{g},\mathbf{u}_t^h\rangle_{\mathcal{F}_h^N}. \tag{35}$$

Step 2. We consider the DG approximation of equation (6b) differentiated with respect to time

$$\left(\mathcal{A}\boldsymbol{\sigma}_t^h - \boldsymbol{\varepsilon}(\mathbf{u}_t^h), \boldsymbol{\tau}\right)_{\mathcal{T}_h} + \langle\{\widehat{\mathbf{u}}_t - \mathbf{u}_t^h\}, [\![\boldsymbol{\tau}]\!]\rangle_{\mathcal{F}_h^o} + \left\langle [\![\widehat{\mathbf{u}}_t - \mathbf{u}_t^h]\!], \{\boldsymbol{\tau}\}\right\rangle_{\mathcal{F}_h^o\cup\mathcal{F}_h^D} + \left\langle \mathbf{c}_{22}(\boldsymbol{\sigma}_t^h\mathbf{n} - \mathbf{g}_t), \boldsymbol{\tau}\,\mathbf{n}\right\rangle_{\mathcal{F}_h^N} = 0$$

for all $\boldsymbol{\tau} \in \boldsymbol{\Sigma}_h$, where the numerical flux $\widehat{\mathbf{u}}_t$ is defined according to the definition of $\widehat{\mathbf{u}}$. In particular on boundary faces we have $\widehat{\mathbf{u}}_t = \mathbf{0}$ on Γ_D. By setting $\boldsymbol{\tau} = \boldsymbol{\sigma}^h$ in the above equation, and using that $[\![\widehat{\mathbf{u}}_t]\!] = \mathbf{0}$ we get,

$$\left(\mathcal{A}\boldsymbol{\sigma}_t^h - \boldsymbol{\varepsilon}(\mathbf{u}_t^h), \boldsymbol{\sigma}^h\right)_{\mathcal{T}_h} - \langle\{\widehat{\mathbf{u}}_t - \mathbf{u}_t^h\}, [\![\boldsymbol{\sigma}_h\,]\!]\rangle_{\mathcal{F}_h^o} + \left\langle [\![\mathbf{u}_t^h]\!], \{\boldsymbol{\sigma}^h\}\right\rangle_{\mathcal{F}_h^o\cup\mathcal{F}_h^D} + \left\langle \mathbf{c}_{22}\boldsymbol{\sigma}_t^h, \boldsymbol{\sigma}^h\,\mathbf{n}\right\rangle_{\mathcal{F}_h^N} = \langle\mathbf{c}_{22}\mathbf{g}_t, \boldsymbol{\sigma}^h\,\mathbf{n}\rangle_{\mathcal{F}_h^N}.$$

Step 3. Summing up the above equation and (35) we have

$$\left(\rho\mathbf{u}_{tt}^h, \mathbf{u}_t^h\right)_{\mathcal{T}_h} + \left(\mathcal{A}\boldsymbol{\sigma}_t^h, \boldsymbol{\sigma}^h\right)_{\mathcal{T}_h} + \mathcal{Q} = \left(\mathbf{f}, \mathbf{u}_t^h\right)_{\mathcal{T}_h} + \left\langle\mathbf{g}, \mathbf{u}_t^h\right\rangle_{\mathcal{F}_h^N} + \langle\mathbf{c}_{22}\mathbf{g}_t, \boldsymbol{\sigma}^h\,\mathbf{n}\rangle_{\mathcal{F}_h^N}, \tag{36}$$

where $\mathcal{Q}$ is defined by

$$\mathcal{Q} = -\langle\{\widehat{\boldsymbol{\sigma}}\}, [\![\mathbf{u}_t^h]\!]\rangle_{\mathcal{F}_h^o\cup\mathcal{F}_h^D} + \left\langle [\![\mathbf{u}_t^h]\!], \{\boldsymbol{\sigma}^h\}\right\rangle_{\mathcal{F}_h^o\cup\mathcal{F}_h^D} - \langle\{\widehat{\mathbf{u}}_t - \mathbf{u}_t^h\}, [\![\boldsymbol{\sigma}^h\,]\!]\rangle_{\mathcal{F}_h^o} + \left\langle \mathbf{c}_{22}\boldsymbol{\sigma}_t^h, \boldsymbol{\sigma}^h\right\rangle_{\mathcal{F}_h^N}. \tag{37}$$

Equation (36) is then equivalent to

$$\frac{1}{2}\frac{d}{dt}\left(\|\rho^{1/2}\mathbf{u}_t^h\|^2_{0,\mathcal{T}_h} + \|\mathcal{A}^{1/2}\boldsymbol{\sigma}^h\|^2_{0,\mathcal{T}_h}\right) + \mathcal{Q} = (\mathbf{f},\mathbf{u}_t^h)_{\mathcal{T}_h} + \langle\mathbf{g},\mathbf{u}_t^h\rangle_{\mathcal{F}_h^N} + \langle\mathbf{c}_{22}\mathbf{g}_t,\boldsymbol{\sigma}^h\,\mathbf{n}\rangle_{\mathcal{F}_h^N}. \tag{38}$$

We first study the case (i), i.e., $\mathbf{f} = \mathbf{g} = \mathbf{0}$. Then to guarantee stability of the method it is enough to show that $\mathcal{Q}$ is either non-negative or it can be rewritten as the time derivative of a non-negative quantity. Substituting in (37) the definition of the fluxes (20) for the FDG methods, $\mathcal{Q}$ becomes

$$\begin{aligned}\mathcal{Q}^{FDG} = &-\left\langle \{\boldsymbol{\sigma}^h\}_\delta - \{\boldsymbol{\sigma}^h\}, [\![\mathbf{u}_t^h]\!] \right\rangle_{\mathcal{F}_h^o \cup \mathcal{F}_h^D} + \left\langle \mathbf{c}_{11}[\![\mathbf{u}^h]\!], [\![\mathbf{u}_t^h]\!] \right\rangle_{\mathcal{F}_h^o \cup \mathcal{F}_h^D} \\ &+ \left\langle \{\mathbf{u}_t^h\} - \{\mathbf{u}_t^h\}_{1-\delta}, [\![\boldsymbol{\sigma}^h]\!] \right\rangle_{\mathcal{F}_h^o} + \left\langle \mathbf{c}_{22}[\![\boldsymbol{\sigma}_t^h]\!], [\![\boldsymbol{\sigma}^h]\!] \right\rangle_{\mathcal{F}_h^o} + \left\langle \mathbf{c}_{22}\boldsymbol{\sigma}_t^h, \boldsymbol{\sigma}^h \right\rangle_{\mathcal{F}_h^N}.\end{aligned}$$

Thanks to the definition of the average operator on boundary edges/faces and the identity (13) with $\boldsymbol{\tau} = \boldsymbol{\sigma}^h$ and $\mathbf{v} = \mathbf{u}_t^h$, we have

$$\langle \{\boldsymbol{\sigma}^h\}_\delta - \{\boldsymbol{\sigma}^h\}, [\![\mathbf{u}_t^h]\!] \rangle_{\mathcal{F}_h^o \cup \mathcal{F}_h^D} = \langle \{\mathbf{u}_t^h\} - \{\mathbf{u}_t^h\}_{1-\delta}, [\![\boldsymbol{\sigma}^h]\!] \rangle_{\mathcal{F}_h^o}, \tag{39}$$

and therefore

$$\mathcal{Q}^{FDG} = \frac{1}{2}\frac{d}{dt}\left(\|\mathbf{c}_{11}^{1/2}[\![\mathbf{u}^h]\!]\|^2_{0,\mathcal{F}_h^o \cup \mathcal{F}_h^D} + \|\mathbf{c}_{22}^{1/2}[\![\boldsymbol{\sigma}^h]\!]\|^2_{0,\mathcal{F}_h^o \cup \mathcal{F}_h^N} \right). \tag{40}$$

For the LDG ($\mathbf{c}_{22} = \mathbf{0}$) and the ALT ($\mathbf{c}_{11} = \mathbf{c}_{22} = \mathbf{0}$) methods the above expression reduces to

$$\mathcal{Q}^{LDG} = \frac{1}{2}\frac{d}{dt}\left\| \mathbf{c}_{11}^{1/2}[\![\mathbf{u}^h]\!] \right\|^2_{0,\mathcal{F}_h^o \cup \mathcal{F}_h^D}, \qquad \mathcal{Q}^{ALT} = 0.$$

Therefore, for all the considered methods, the corresponding discrete energy defined in (28) is preserved in time.

Next we deal with the case *(ii)*. By using estimate (31) from Lemma 1, we find

$$\left\| (\mathbf{u}^h, \boldsymbol{\sigma}^h) \right\|^2_{\mathcal{E},\mathrm{MDG}} \lesssim \left\| (\mathbf{u}_0^h, \boldsymbol{\sigma}_0^h) \right\|^2_{\mathcal{E},\mathrm{MDG}} + 2\int_0^t \rho_*^{-1/2} \|\mathbf{f}\|_{0,\Omega} \|\rho^{1/2}\mathbf{u}_\tau^h\|_{0,\mathcal{T}_h} d\tau,$$

which together with the definition (28) and Gronwall's lemma [42, p 28] gives the result and proves part (ii). We finally show part (iii).

We consider the FDG formulation; the corresponding estimate for the LDG can be obtained by setting $\mathbf{c}_{22} = \mathbf{0}$. Substituting (40) into (38) gives

$$\begin{aligned}&\frac{1}{2}\frac{d}{dt}\left(\|\rho^{1/2}\mathbf{u}_t^h\|^2_{0,\mathcal{T}_h} + \|\mathcal{A}^{1/2}\boldsymbol{\sigma}^h\|^2_{0,\mathcal{T}_h} + \|\mathbf{c}_{11}^{1/2}[\![\mathbf{u}^h]\!]\|^2_{0,\mathcal{F}_h^o \cup \mathcal{F}_h^D} + \|\mathbf{c}_{22}^{1/2}[\![\boldsymbol{\sigma}^h]\!]\|^2_{0,\mathcal{F}_h^o \cup \mathcal{F}_h^N} \right) \\ &\quad = (\mathbf{f}, \mathbf{u}_t^h)_{\mathcal{T}_h} + \langle \mathbf{g}, \mathbf{u}_t^h \rangle_{\mathcal{F}_h^N} + \langle \mathbf{c}_{22}\mathbf{g}_t, \boldsymbol{\sigma}^h\, \mathbf{n} \rangle_{\mathcal{F}_h^N}.\end{aligned} \tag{41}$$

Recalling now the definition of the $\|\cdot\|_{\mathcal{E},\mathrm{MDG}}$ norm (28), and integrating in time we get

$$\begin{aligned}\frac{1}{2}\left\| (\mathbf{u}^h, \boldsymbol{\sigma}^h)(t) \right\|^2_{\mathcal{E},\mathrm{MDG}} \le \frac{1}{2}\left\| (\mathbf{u}_0^h, \boldsymbol{\sigma}_0^h) \right\|^2_{\mathcal{E},\mathrm{MDG}} &+ \underbrace{\left| \int_0^t (\mathbf{f}, \mathbf{u}_\tau^h)_{\mathcal{T}_h}\, d\tau \right|}_{\mathrm{I}} \\ &+ \underbrace{\left| \int_0^t \langle \mathbf{g}, \mathbf{u}_\tau^h \rangle_{\mathcal{F}_h^N}\, d\tau \right|}_{\mathrm{II}} + \underbrace{\left| \int_0^t \langle \mathbf{c}_{22}\mathbf{g}_\tau, \boldsymbol{\sigma}^h\, \mathbf{n} \rangle_{\mathcal{F}_h^N}\, d\tau \right|}_{\mathrm{III}}.\end{aligned}$$

The terms I and III are readily estimated by using Lemma 1

$$\mathrm{I} \leq \int_0^t \rho_*^{-1/2} \|\mathbf{f}\|_{0,\Omega} \|\rho^{1/2}\mathbf{u}_\tau^h\|_{0,\mathcal{T}_h}\, d\tau,$$
$$\mathrm{III} \lesssim \int_0^t \mathrm{D}_*^{-1/2} \|\mathbf{g}_\tau\|_{1/2,\Gamma_N} \|\mathbf{c}_{22}^{1/2}\boldsymbol{\sigma}^h\mathbf{n}\|_{0,\mathcal{F}_h^N}\, d\tau\ .$$

To estimate the term II, from Lemma 1 we first have for any $\epsilon > 0$ (to be specified later)

$$\mathrm{II} \lesssim \epsilon \left\|\mathbf{u}^h\right\|_a^2 + \left\|\mathbf{u}_0^h\right\|_a \|\mathbf{g}_0\|_{1,\Gamma_N} + \frac{\mathrm{D}_*^{-1}}{\epsilon}\|\mathbf{g}\|_{1,\Gamma_N}^2 + \int_0^t \mathrm{D}_*^{-1/2}\|\mathbf{g}_\tau\|_{1,\Gamma_N}\left\|\mathbf{u}^h\right\|_a d\tau.$$

Now, to bound $\left\|\mathbf{u}^h\right\|_a$ in terms of the $\left\|(\mathbf{u}^h,\boldsymbol{\sigma}^h)\right\|_{\mathcal{E},\mathrm{MDG}}$ norm, we use estimate (34) from Lemma 2, to get

$$\left\|\mathbf{u}^h\right\|_a^2 \leq C_{\mathrm{II}}\left(\left\|(\mathbf{u}^h,\boldsymbol{\sigma}^h)\right\|_{\mathcal{E},\mathrm{MDG}}^2 + \mathrm{D}_*^{-1}\|\mathbf{g}\|_{1/2,\Gamma_N}^2\right),$$

and so the estimate for the term II becomes,

$$\mathrm{II} \lesssim \epsilon C_{\mathrm{II}}\left\|(\mathbf{u}^h,\boldsymbol{\sigma}^h)\right\|_{\mathcal{E},\mathrm{MDG}}^2 + \left\|\mathbf{u}_0^h\right\|_a\|\mathbf{g}_0\|_{1,\Gamma_N} + \frac{\mathrm{D}_*^{-1}}{\epsilon}\|\mathbf{g}\|_{1,\Gamma_N}^2 + \epsilon C_{\mathrm{II}}\mathrm{D}_*^{-1}\|\mathbf{g}\|_{1/2,\Gamma_N}^2$$
$$+ \int_0^t \mathrm{D}_*^{-1/2}\|\mathbf{g}_\tau\|_{1,\Gamma_N}\left\|(\mathbf{u}^h,\boldsymbol{\sigma}^h)\right\|_{\mathcal{E},\mathrm{MDG}} d\tau + \int_0^t \mathrm{D}_*^{-1}\|\mathbf{g}_\tau\|_{1,\Gamma_N}\|\mathbf{g}\|_{1/2,\Gamma_N}\, d\tau$$

Substituting all the above estimates, recalling the definition of the $\|\cdot\|_{\mathcal{E},\mathrm{MDG}}$ norm, using standard Sobolev embeddings and taking ϵ so that $1/2 - C_{\mathrm{II}}\epsilon$ is positive, gives

$$\left\|(\mathbf{u}^h,\boldsymbol{\sigma}^h)\right\|_{\mathcal{E},\mathrm{MDG}}^2 \lesssim \left\|(\mathbf{u}_0^h,\boldsymbol{\sigma}_0^h)\right\|_{\mathcal{E},\mathrm{MDG}}^2 + \mathrm{D}_*^{-1/2}\left\|\mathbf{u}_0^h\right\|_a\|\mathbf{g}_0\|_{1,\Gamma_N}$$
$$+\mathrm{D}_*^{-1}\|\mathbf{g}\|_{1,\Gamma_N}^2 + \int_0^t \mathrm{D}_*^{-1}\|\mathbf{g}_\tau\|_{1,\Gamma_N}\|\mathbf{g}\|_{1/2,\Gamma_N}\, d\tau$$
$$+\int_0^t\left(\rho_*^{-1/2}\|\mathbf{f}\|_{0,\Omega} + \mathrm{D}_*^{-1/2}\|\mathbf{g}_\tau\|_{1,\Gamma_N}\right)\left\|(\mathbf{u}^h,\boldsymbol{\sigma}^h)\right\|_{\mathcal{E},\mathrm{MDG}} d\tau.$$

By a standard application of Gronwall's lemma [42, p. 28] the proof now follows. □

Before proving Proposition 2 we first observe that, for any $F \in \mathcal{F}_h^o \cup \mathcal{F}_h^D$, and any $\mathbf{w}, \mathbf{v} \in \boldsymbol{V}_h$, the Cauchy–Schwarz, Agmon inequality (14) and inverse inequality (18) give

$$|\langle\{\mathcal{D}\boldsymbol{\varepsilon}(\mathbf{w})\}_\delta, [\![\mathbf{v}]\!]\rangle_F| \lesssim \frac{1}{\mathbf{c}_{00}}\|\mathcal{D}^{1/2}\boldsymbol{\varepsilon}(\mathbf{w})\|_{0,K}\|\mathbf{S}_F^{1/2}[\![\mathbf{v}]\!]\|_{0,F}^2 \leq \frac{1}{\mathbf{c}_{00}}\|\mathbf{w}\|_{\mathcal{E},\mathrm{IP}}\|\mathbf{v}\|_{\mathcal{E},\mathrm{IP}} \tag{42}$$

where $\mathbf{c}_{00}$ is the positive parameter appearing in the definition of the penalty function (25).

Proof (Proof of Proposition 2) The proof is obtained as follows.
Step 1. We set $\mathbf{v} = \mathbf{u}_t^h \in \boldsymbol{V}_h$ in (26) to get

$$\frac{1}{2}\frac{d}{dt}\left(\left\|\mathbf{u}^h\right\|_{\mathcal{E},\mathrm{IP}}^2 - 2\langle\{\mathcal{D}\boldsymbol{\varepsilon}(\mathbf{u}^h)\}_\delta, [\![\mathbf{u}^h]\!]\rangle_{\mathcal{F}_h^o\cup\mathcal{F}_h^D}\right) = (\mathbf{f},\mathbf{u}_t^h)_{\mathcal{T}_h} + \langle\mathbf{g},\mathbf{u}_t^h\rangle_{\mathcal{F}_h^N}. \tag{43}$$

Step 2. Integrating in time the above equation we obtain

$$\left\|\mathbf{u}^h\right\|_{\mathcal{E},\mathrm{IP}}^2 - 2\langle\{\mathcal{D}\boldsymbol{\varepsilon}(\mathbf{u}^h)\}_\delta, [\![\mathbf{u}^h]\!]\rangle_{\mathcal{F}_h^o\cup\mathcal{F}_h^D} = \left\|\mathbf{u}_0^h\right\|_{\mathcal{E},\mathrm{IP}}^2 - 2\langle\{\mathcal{D}\boldsymbol{\varepsilon}(\mathbf{u}_0^h)\}_\delta, [\![\mathbf{u}_0^h]\!]\rangle_{\mathcal{F}_h^o\cup\mathcal{F}_h^D}$$
$$+2\int_0^t(\mathbf{f},\mathbf{u}_\tau^h)_{\mathcal{T}_h}\, d\tau + 2\int_0^t\langle\mathbf{g},\mathbf{u}_\tau^h\rangle_{\mathcal{F}_h^N}\, d\tau. \tag{44}$$

Using (42), the arithmetic-geometric inequality and choosing the penalty parameter $\mathbf{c}_{00}$ sufficiently large, we obtain

$$\left\|\mathbf{u}^h\right\|^2_{\mathcal{E},\mathrm{IP}} - 2\langle\{\mathcal{D}\boldsymbol{\varepsilon}(\mathbf{u}^h)\}_\delta, [\![\mathbf{u}^h]\!]\rangle_{\mathcal{F}_h^o\cup\mathcal{F}_h^D} \gtrsim \left\|\mathbf{u}^h\right\|^2_{\mathcal{E},\mathrm{IP}},$$
$$\left\|\mathbf{u}_0^h\right\|^2_{\mathcal{E},\mathrm{IP}} - 2\langle\{\mathcal{D}\boldsymbol{\varepsilon}(\mathbf{u}_0^h)\}_\delta, [\![\mathbf{u}^h(0)]\!]\rangle_{\mathcal{F}_h^o\cup\mathcal{F}_h^D} \lesssim \left\|\mathbf{u}_0^h\right\|^2_{\mathcal{E},\mathrm{IP}}.$$

Substituting now these two estimates into (44), gives

$$\left\|\mathbf{u}^h\right\|^2_{\mathcal{E},\mathrm{IP}} \lesssim \left\|\mathbf{u}_0^h\right\|^2_{\mathcal{E},\mathrm{IP}} + \int_0^t (\mathbf{f}, \mathbf{u}_\tau^h)_{\mathcal{T}_h}\, d\tau + \int_0^t \langle \mathbf{g}, \mathbf{u}_\tau^h\rangle_{\mathcal{F}_h^N}\, d\tau.$$

If $\mathbf{f} = \mathbf{g} = \mathbf{0}$, part (i) of the thesis follows. As regards part (ii), Lemma 1 and the inequality $\left\|\mathbf{u}^h\right\|_a \le \left\|\mathbf{u}^h\right\|_{\mathcal{E},\mathrm{IP}}$, give for $\epsilon > 0$

$$\left\|\mathbf{u}^h\right\|^2_{\mathcal{E},\mathrm{IP}} \lesssim \epsilon \left\|\mathbf{u}^h\right\|^2_{\mathcal{E},\mathrm{IP}} + \left\|\mathbf{u}_0^h\right\|^2_{\mathcal{E},\mathrm{IP}} + \left\|\mathbf{u}_0^h\right\|_a \|\mathbf{g}_0\|_{1,\Gamma_N}$$
$$+ \frac{\mathrm{D}_*^{-1}}{\epsilon}\|\mathbf{g}\|^2_{1,\Gamma_N} + \int_0^t \left(\rho_*^{-1}\|\mathbf{f}\|_{0,\Omega} + \mathrm{D}_*^{-1/2}\|\mathbf{g}_\tau\|_{1,\Gamma_N}\right)\left\|\mathbf{u}^h\right\|_{\mathcal{E},\mathrm{IP}} d\tau.$$

Choosing ϵ small enough we obtain

$$\left\|\mathbf{u}^h\right\|^2_{\mathcal{E},\mathrm{IP}} \lesssim \left\|\mathbf{u}_0^h\right\|^2_{\mathcal{E},\mathrm{IP}} + \left\|\mathbf{u}_0^h\right\|_a \|\mathbf{g}_0\|_{1,\Gamma_N} + \mathrm{D}_*^{-1}\|\mathbf{g}\|^2_{1,\Gamma_N}$$
$$+ \int_0^t \left(\rho_*^{-1}\|\mathbf{f}\|_{0,\Omega} + \mathrm{D}_*^{-1/2}\|\mathbf{g}_\tau\|_{1,\Gamma_N}\right)\left\|\mathbf{u}^h\right\|_{\mathcal{E},\mathrm{IP}} d\tau,$$

and *(ii)* follows by a standard application of Gronwall's lemma [42, p. 28]. □

6 Error Analysis

In this section we state the *a priori* error estimates for the DG methods introduced in Sect. 4. The proof follows from the stability results by using standard arguments (see [2] for detailed proofs). For $(\mathbf{v}, \boldsymbol{\sigma}) \in C^2((0,T]; \mathbf{H}^1(\mathcal{T}_h) \cap \mathbf{H}^2(\mathcal{T}_h)) \times C^0((0,T]; \boldsymbol{\mathcal{H}}^1(\mathcal{T}_h))$ we introduce the following augmented norms

$$|||(\mathbf{v}, \boldsymbol{\sigma})|||^2_{\mathcal{E},\mathrm{MDG}} = \|(\mathbf{v}, \boldsymbol{\sigma})\|^2_{\mathcal{E},\mathrm{MDG}} + \left\|\mathbf{c}_{22}^{1/2}\{\boldsymbol{\sigma}\}_\delta\right\|^2_{0,\mathcal{F}_h^o\cup\mathcal{F}_h^D},$$
$$|||\mathbf{v}|||^2_{\mathcal{E},\mathrm{IP}} = \|\mathbf{v}\|^2_{\mathcal{E},\mathrm{IP}} + \left\|h_F^{1/2}\{\mathcal{D}\boldsymbol{\varepsilon}(\mathbf{v})\}_\delta\right\|^2_{0,\mathcal{F}_h^o\cup\mathcal{F}_h^D},$$

where $\|(\cdot,\cdot)\|_{\mathcal{E},\mathrm{MDG}}$ and $\|\cdot\|_{\mathcal{E},\mathrm{IP}}$ are defined in (28) and (29), respectively.

Theorem 1 *Let* $(\mathbf{u}, \boldsymbol{\sigma})$ *be the solution of* (6a)–(6b) *and let* $(\mathbf{u}^h, \boldsymbol{\sigma}^h) \in C^2((0,T]; \boldsymbol{V}_h) \times C^0((0,T]; \boldsymbol{\Sigma}_h)$ *be the solution of any of the DG method in displacement-stress formulations defined in Sect. 4. Then,*

$$\sup_{0<t\le T} \left\|(\mathbf{u}(t) - \mathbf{u}^h(t), \boldsymbol{\sigma}(t) - \boldsymbol{\sigma}^h(t))\right\|_{\mathcal{E},MDG}$$
$$\lesssim h^k \sup_{0<t\le T} \left(|\mathbf{u}(t)|^2_{k+1,\Omega} + h^2|\boldsymbol{\sigma}(t)|^2_{k+1,\Omega} + h^2|\mathbf{u}_\tau(t)|_{k+1,\Omega}\right)^{1/2}$$

$$+h^k \int_0^T \left(|\mathbf{u}(\tau)|^2_{k+1,\Omega} + h^2|\boldsymbol{\sigma}(\tau)|^2_{k+1,\Omega} + h^2|\mathbf{u}_\tau(\tau)|_{k+1,\Omega}\right)^{1/2} d\tau$$
$$+h^k \int_0^T \left(|\mathbf{u}_\tau(\tau)|^2_{k+1,\Omega} + h^2|\boldsymbol{\sigma}_\tau(\tau)|^2_{k+1,\Omega} + h^2|\mathbf{u}_{\tau\tau}(\tau)|_{k+1,\Omega}\right)^{1/2} d\tau, \quad (45)$$

where the hidden constant depends on D_*, D^*, ρ^*, *k, and the shape regularity constant of* $\mathcal{T}_h$.

For displacement formulations we proceed similarly and obtain the following *a-priori* estimate.

Theorem 2 *Let* $\mathbf{u}$ *be the solution of* (7)*, and let* $\mathbf{u}^h \in C^2((0,T];\boldsymbol{V}_h)$ *be the approximated solution obtained with the SIP(*δ*) method defined in Sect. 5. Assume that the penalty parameter* $\mathbf{c}_{00}$ *appearing in* (25) *is large enough. Then,*

$$\sup_{0<t\leq T} \left\|\mathbf{u}(t) - \mathbf{u}^h(t)\right\|_{\mathcal{E},IP} \lesssim h^k \sup_{0<t\leq T} \left(|\mathbf{u}(t)|^2_{k+1,\Omega} + h^2|\mathbf{u}_\tau(t)|^2_{k+1,\Omega}\right)^{1/2}$$
$$+h^k \int_0^T \left(|\mathbf{u}_\tau(\tau)|^2_{k+1,\Omega} + h^2|\mathbf{u}_{\tau\tau}(\tau)|^2_{k+1,\Omega}\right)^{1/2} d\tau, \quad (46)$$

where the hidden constant depends on k, D^*, ρ^*, *and the shape regularity constant of the mesh* $\mathcal{T}_h$.

7 Numerical Results

To conclude our analysis we present some numerical results. The fully discrete solution is recovered by combining our semidiscrete formulation with the second order accurate explicit leap-frog time integration scheme, where the integration time-step has be chosen sufficiently small in order to guarantee that the temporal component of the error does not affect the spatial one.

7.1 Two Dimensional Test Case

We set $\Omega = (0,1)^2$, $\Gamma_D = \partial\Omega$, $\lambda = \mu = \rho = 1$ and choose $\mathbf{f}$ so that the analytical solution for the problem (6a)–(6b) is given by

$$\mathbf{u}(\mathbf{x},t) = \sin(\sqrt{2}\pi t)\begin{bmatrix} \sin(\pi x)^2 \sin(2\pi y) \\ -\sin(2\pi x)\sin(\pi y)^2 \end{bmatrix}.$$

The Dirichlet boundary conditions on the whole $\partial\Omega$, the initial displacement $\mathbf{u}_0$, and initial velocity $\mathbf{u}_1$ have been set accordingly. The computations reported in this section have been obtained using the finite element software `FreeFem++`, cf. [23]. We test our DG schemes on a sequence of successively refined triangular meshes with mesh size $h = 0.25, 0.125, 0.0625, 0.03125$ and consider a polynomial approximation degree $k = 1, 2$.

We start comparing the approximation properties of the LDG ($\mathbf{c}_{11} = 10$) and the SIP ($\mathbf{c}_{00} = 10$) methods, cf. Sect. 4. We have ran the same set of experiments with the ALT method, cf. Sect. 4, and a completely analogous behavior has been observed; for brevity such results have been omitted. For the sake of comparison, we have also ran the same set of experiments employing the *extra-stabilized* Non-symmetric Interior Penalty (sNIP) method

Table 1 Computed errors measured in the corresponding energy norm as a function of the mesh size h for linear ($k = 1$) and quadratic ($k = 2$) finite element, and corresponding computed convergence rates (last line)

	E_{SIP}		E_{LDG}		E_{sNIP} [47]	
h	k = 1	k = 2	k = 1	k = 2	k = 1	k = 2
0.25000	2.7950	0.8767	3.3471	0.9212	2.7968	0.8772
0.12500	1.6364	0.2528	1.8803	0.2650	1.6366	0.2529
0.06250	0.8575	0.0669	0.9405	0.0704	0.8575	0.0669
0.03125	0.4338	0.0174	0.4639	0.0180	0.4337	0.0171
Rate	0.9832	1.9398	1.0197	1.9701	0.9833	1.9650

described in [45] (cf. also in [39,46,47]) that reads as: find $\mathbf{u}^h \in \boldsymbol{V}_h$ such that for all $\mathbf{v} \in \boldsymbol{V}_h$ it holds

$$\begin{aligned}
&\left(\rho \mathbf{u}^h_{tt}, \mathbf{v}\right)_{\mathcal{T}_h} + (\boldsymbol{\varepsilon}(\mathbf{u}^h), \mathcal{D}\boldsymbol{\varepsilon}(\mathbf{v}))_{\mathcal{T}_h} - \langle \{\mathcal{D}\boldsymbol{\varepsilon}(\mathbf{u}^h)\}_\delta, [\![\mathbf{v}]\!] \rangle_{\mathcal{F}_h^o \cup \mathcal{F}_h^D} \\
&+ \langle [\![\mathbf{u}^h]\!], \{\mathcal{D}\boldsymbol{\varepsilon}(\mathbf{v})\}_\delta \rangle_{\mathcal{F}_h^o \cup \mathcal{F}_h^D} + \langle \mathbf{S}_F [\![\mathbf{u}^h]\!], [\![\mathbf{v}]\!] \rangle_{\mathcal{F}_h^o \cup \mathcal{F}_h^D} \\
&+ \langle \mathbf{S}_F [\![\mathbf{u}^h_t]\!], [\![\mathbf{v}]\!] \rangle_{\mathcal{F}_h^o \cup \mathcal{F}_h^D} = (\mathbf{f}, \mathbf{v})_{\mathcal{T}_h} + \langle \mathbf{g}, \mathbf{v} \rangle_{\mathcal{F}_h^N},
\end{aligned} \tag{47}$$

where the extra stabilization term is required for ensuring (at the theoretical level) the stability of the method. For the sNIP scheme we measured the error in the following norm:

$$\left\| \mathbf{u}^h(t) \right\|^2_{\mathcal{E},\text{sNIP}} = \left\| \mathbf{u}^h(t) \right\|^2_{\mathcal{E},\text{IP}} + \left\| \mathbf{S}_F^{1/2} [\![\mathbf{u}^h_t(t)]\!] \right\|^2_{0,\mathcal{F}_h^o \cup \mathcal{F}_h^D}.$$

The simulations have been performed setting $T = 10$, and a time step $\Delta t = 1 \cdot 10^{-4}$. The corresponding energy norms have been evaluated at each discrete time $t_n = t_0 + n\Delta t$, for $n = 1, \ldots, 10^5$, and we measured the quantities

$$\begin{aligned}
E_{\text{LDG}} &= \max_{0<t_n\le T} \left\| (\mathbf{u}(t_n) - \mathbf{u}^h(t_h), \boldsymbol{\sigma}(t_h) - \boldsymbol{\sigma}^h(t_h)) \right\|_{\mathcal{E},\text{LDG}}, \\
E_{\text{IP}} &= \max_{0<t_n\le T} \|\mathbf{u}(t_n) - \mathbf{u}^h(t_n)\|_{\mathcal{E},\text{IP}}, \\
E_{\text{sNIP}} &= \max_{0<t_n\le T} \|\mathbf{u}(t_n) - \mathbf{u}^h(t_n)\|_{\mathcal{E},\text{sNIP}},
\end{aligned} \tag{48}$$

which represent good approximation of the quantities estimated in Theorem 1 and Theorem 2, respectively, at least when the time discretization error is small compared to the spatial one. In Table 1 we report the computed errors measured in the corresponding energy norm as a function the mesh size h for linear ($k = 1$) and quadratic ($k = 2$) finite elements; in the last row of Table 1 the estimated convergence rate is also reported. The results confirm the expected convergence rate proved in Theorem 1 and Theorem 2 for the LDG and SIP methods, respectively, *i.e.*, the error decreases linearly (resp. quadratically) as a function of the mesh size when linear (resp. quadratic) polynomials are employed. We also observe that the sNIP scheme exhibits the same order of accuracy of the SIP and LDG methods, in agreement with [47, Theorem 3.1], and that the errors are of the same magnitude than the ones computed with the other DG schemes.

Next, we compare the accuracy of the SIP and LDG as a function of the total number of degrees of freedom. More precisely, in Fig. 1 we report the computed errors as a function of the total number of degrees of freedom (semilog scale) for the SIP and LDG methods and for $k = 1, 2$. From the results shown in Fig. 1, it is clear that the SIP scheme achieves

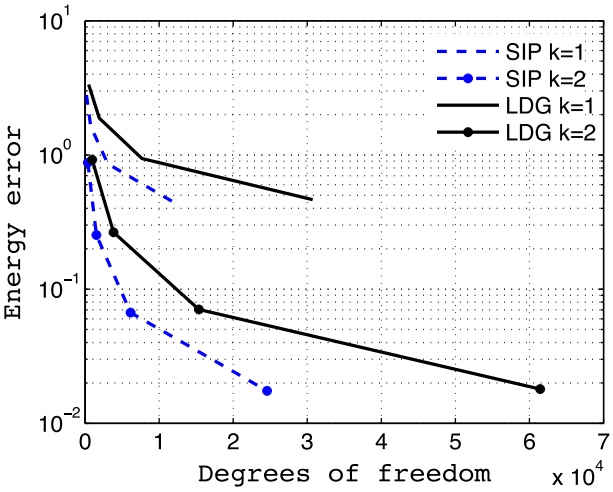

Fig. 1 Computed errors measured in the corresponding energy norm as a function of the total number of degrees of freedom for linear ($k = 1$) and quadratic ($k = 2$) finite elements (semilog scale)

the same accuracy of the LDG methods using less than a half degrees of freedom. From a computational point of view this is the main drawback of *displacement-stress* based methods with respect to the *displacement* based ones. This shortcoming becomes crucial in three dimensions where the number unknowns should be kept as low as possible in order to keep the computational cost under control.

7.2 Three Dimensional Test Case

We solve a wave propagation problem in $\Omega = (0, 1)^3$, set the Lamé parameters λ, μ and the mass density ρ equal to 1, and choose $\mathbf{f}$ such that problem (7) features the exact solution

$$\mathbf{u}(\mathbf{x}, t) = \sin(3\pi t) \begin{bmatrix} -\sin^2(\pi x)\sin(2\pi y)\sin(2\pi z) \\ \sin(2\pi x)\sin^2(\pi y)\sin(2\pi z) \\ \sin(2\pi x)\sin(2\pi y)\sin^2(\pi z) \end{bmatrix}.$$

The Dirichlet boundary conditions on the whole $\partial\Omega$, the initial displacement $\mathbf{u}_0$, and initial velocity $\mathbf{u}_1$ have been set accordingly. The numerical computation reported in this section have been obtained using the DG spectral element code SPEED (http://speed.mox.polimi.it), cf. [35]. For brevity, in this section we focus only on DG methods for the *displacement* formulation (choosing $\mathbf{c}_{00} = 10$), cf. Sect. 4, since as shown by the numerical results reported in the previous section, it seems that this class of methods is computationally less expensive than *displacement-stress* formulations.

We consider a Cartesian decomposition of the domain Ω and define four levels of refinements with mesh size $h = 0.5, 0.25, 0.125, 0.0625$ (resp. $h = 0.25, 0.125, 0.0625, 0.03125$) for a polynomial approximation degree $k = 2, 3, 4$ (resp. $k = 1$). Since high order spatial approximation of elastodynamics problems have been previously addressed in the context of spectral and spectral element methods, cf. [15,19,20,31,43], we also compared the numerical results obtained with the SIP method with the analogous ones obtained with the spectral element method (SEM). For the spectral element approximation the spatial error has been measured using the energy norm defined in (29), obviously neglecting the last term, since

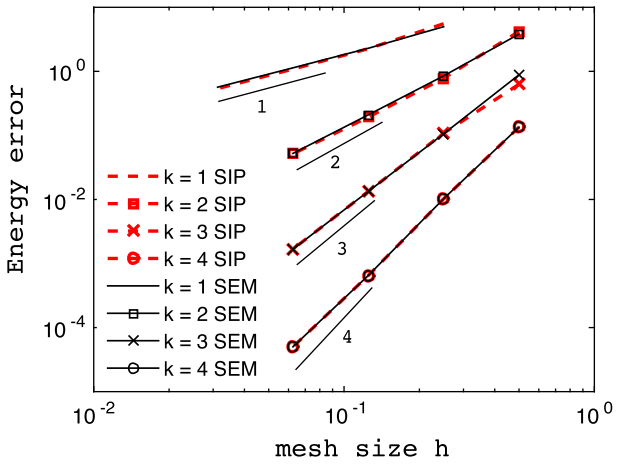

Fig. 2 Computed errors measured in the energy norm versus the mesh size h, for different polynomial approximation degrees $k = 1, 2, 3, 4$ (loglog scale)

Table 2 Computed convergence rates for different approximation degrees $k = 1, 2, 3, 4$

	$k = 1$	$k = 2$	$k = 3$	$k = 4$
SIP	1.1212	2.1157	2.8478	3.7973
SEM	0.9492	2.0622	3.0135	3.7973

the discrete and continuous solutions are continuous across interelement boundaries. The simulations have been carried out setting $T = 10$ and using a time step $\Delta t = 1 \cdot 10^{-5}$. As before, we have computed the maximum of the energy errors evaluated at the discrete times $t_n = t_0 + n\Delta t$, for $n = 1, \ldots, 10^6$. The results of this set of experiments are reported in Fig. 2 where the maximum of the computed errors is plotted versus the mesh size h for different polynomial approximation degrees $k = 1, 2, 3, 4$. The corresponding computed convergence rates are reported in Table 2. The numerical results confirm the theoretical results proved in Theorem 2 and demonstrate once again the $h-$optimality of DG discretizations.

We next investigate the stability of the SIP method and compare it with that of the sNIP method (47) and of the NIP scheme [4] obtained from (47) neglecting the term $\langle \mathbf{S}_F [\![\mathbf{u}_t^h]\!], [\![\mathbf{v}]\!] \rangle_{\mathcal{F}_h^o \cup \mathcal{F}_h^D}$. To provide a consistent comparison, for all the methods the stabilization parameter has been chosen as $\mathbf{c}_{00} = 10$; notice however that sNIP and NIP formulations are stable for any $\mathbf{c}_{00} > 0$. As before, for different Δt, we measured the quantities and E_{SIP} and E_{sNIP}, cf. (48), as well as

$$E_{\text{NIP}} = \max_{0<t_n\leq T} \|\mathbf{u}(t_n) - \mathbf{u}^h(t_n)\|_{\mathcal{E},\text{IP}},$$

where $\mathbf{u}^h$ is the solution computed with the NIP method. In Fig. 3 we show E_{SIP}, E_{sNIP} and E_{NIP} as a function of the time step Δt for different polynomial approximation degrees $k = 1, 2, 3$. The results in Fig. 3 have been obtained with a mesh size $h = 0.125$. Analogous results were obtained for different choices of the mesh size; for brevity these results have been omitted. Clearly, the presence of the additional stabilization term imposes a much severe restriction on the time step size required to guarantee stability, and indeed the SIP and NIP methods seem to have a less restrictive condition than that required by the sNIP scheme, at

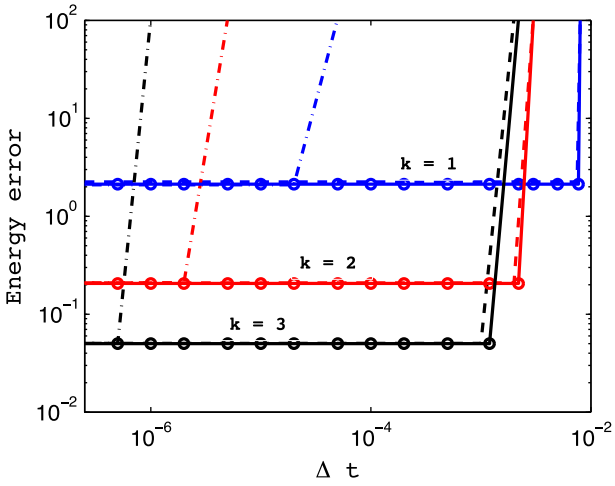

Fig. 3 E_{SIP} (continuous *line with dots*), E_{NIP} (*dash line*) and E_{sNIP} (*dash-dot line*) versus the time step Δt for different polynomial approximation degrees $k = 1, 2, 3$ (loglog scale)

Table 3 Coefficients for the heterogeneous anisotropic model given in $[10^7\ N\,m^{-2}]$ for the anisotropic and isotropic materials

	ρ	$\mathcal{D}_{11}$	$\mathcal{D}_{12}$	$\mathcal{D}_{22}$	$\mathcal{D}_{33}$
Isotropic	2000	5.9858	1.9858	5.9858	2
Anisotropic	2000	5.9858	0.6017	2.2492	2

The material density ρ is given in $[kg\,m^{-3}]$

least when the leap-frog time integration scheme is employed. The simulation uses 2000 time steps of 50 μs. Therefore, despite the fact that the extra term is helpful for the theoretical analysis, it needs to be handled extremely carefully in the numerical simulations, in order to guarantee stability in practice.

7.3 Elastic Wave Propagation in an Anisotropic (Transverly Isotropic) Medium

To further validate the method, we study the elastic wave propagation in a heterogeneous medium. The computational domain $\Omega = (-800, 800)\ \mathrm{m} \times (-400, 400)\ \mathrm{m}$ contains two materials separated by a straight line at $x = 0$. On the right hand side side ($x > 0$) we have an anisotropic (transversely isotropic) body with the symmetry axis in the y-direction, whereas on the left hand side ($x < 0$) we use an isotropic material. Analogous test cases regarding wave propagation in anisotropic media can be found for instance in [10,16,28]. In this case, the stiffness tensor $\mathcal{D}$ has 4 independent components. Using the reduced Voigt notation (see e.g., [24]), Hooke's law (4) becomes

$$\begin{pmatrix}\sigma_{11}\\ \sigma_{22}\\ \sigma_{12}\end{pmatrix} = \begin{pmatrix}\mathcal{D}_{11} & \mathcal{D}_{12} & 0\\ \mathcal{D}_{12} & \mathcal{D}_{22} & 0\\ 0 & 0 & \mathcal{D}_{33}\end{pmatrix}\begin{pmatrix}\epsilon_{11}\\ \epsilon_{22}\\ 2\epsilon_{12}\end{pmatrix}.$$

Then, the isotropic case can be easily obtained by letting $\mathcal{D}_{11} = \mathcal{D}_{22} = \lambda + 2\mu$, $\mathcal{D}_{12} = \lambda$ and $\mathcal{D}_{33} = \mu$. In Table 3 we summarize the mechanical properties considered in this example.

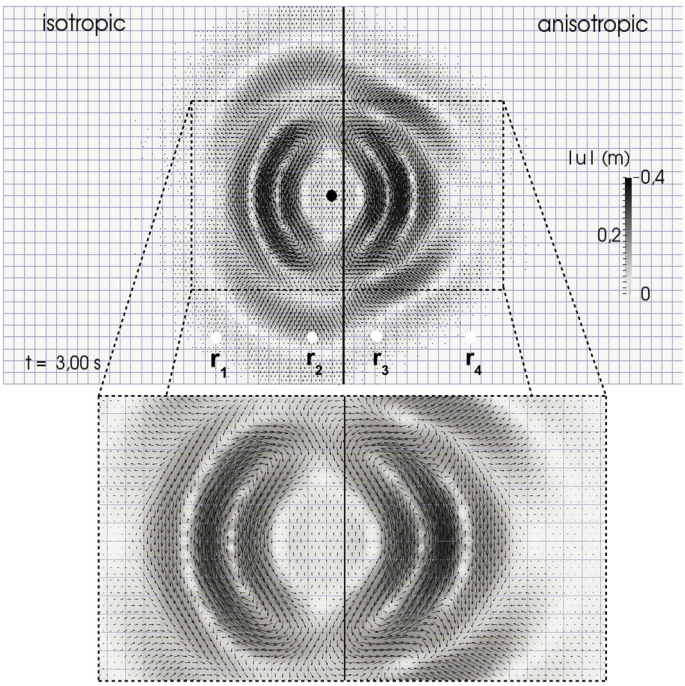

Fig. 4 (*Top*) Displacement field **u** and computational mesh at time $t = 3\,s$. The source location is indicated by a *black circle*, the four receiver locations are indicated by *white circles*. (*Bottom*) Zoom of the displacement field at $t = 3\,s$

The source is represented by a vertical point force located at the point $\mathbf{x}_s = (-25, 0)$ m, that is 25 m from the material interface inside the isotropic material and is acting in the y-direction. The source time function is given by a Ricker wavelet with dominant frequency $f_0 = 2$ Hz and delay $t_0 = 1$ s and amplitude $A = 10^7$ m, that is

$$\mathbf{f}(\mathbf{x}, t) = \left(0, \delta(\mathbf{x} - \mathbf{x}_s) A (1 - 2\pi^2 f_0^2 (t - t_0)^2) e^{-\pi^2 f_0^2 (t-t_0)^2}\right)^T, \tag{49}$$

where $\delta(\cdot)$ is a delta function. Absorbing boundary conditions [4] are used on the four edges of the grid in order to simulate two half-spaces in contact. The displacement field is calculated at four different locations $\mathbf{r}_i = (x_i, y_i)$, $i = 1, \ldots, 4$, with $x_1 = -300$ m, $x_2 = -75$ m, $x_3 = 75$ m, $x_4 = 300$ m and $y_i = -300$ m for all $i = 1, \ldots, 4$. For the spatial discretization we employ the SIP method with sixth order polynomial (with $\mathbf{c}_{00} = 10$) on a Cartesian grid with mesh size 25 m. The time integration is carried out by using the leap-frog scheme and fixing the time step $\Delta t = 1 \cdot 10^{-3}$ s for a total observation time $T = 10$ s. For a quantitative comparison, we perform a SE calculation that is used as a reference with sixth order polynomials and a finer Cartesian grid (size 12.5 m). For a qualitative comparison a snapshot of the displacement field is reported in Fig. 4. The vertical displacement calculated with the SIP scheme at the four receiver locations $\mathbf{r}_i, i = 1, \ldots, 4$, are plotted in Fig. 5 (dashed line). The results obtained by the SE approach with polynomial degree 6 are also reported (solid line). The agreement is very good for all phases.

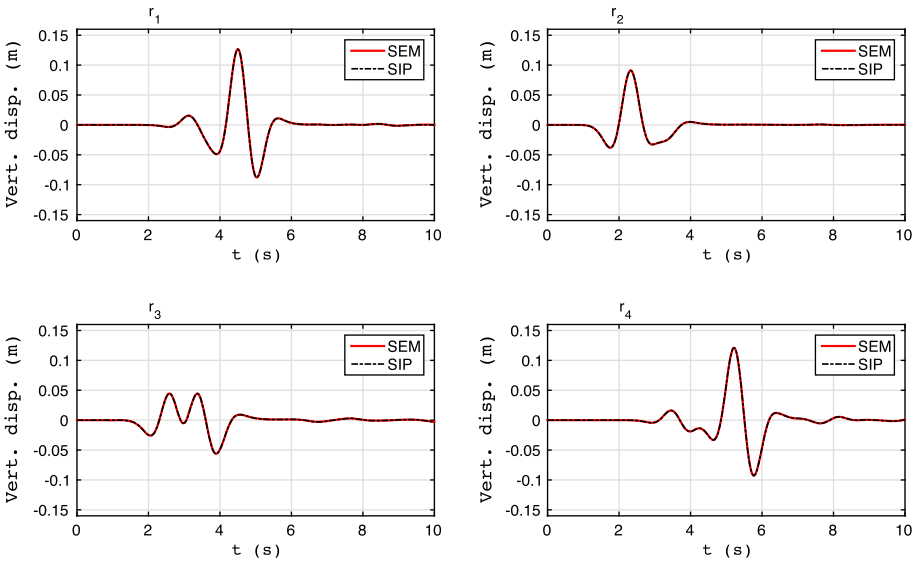

Fig. 5 Vertical displacements for the SIP (*dashed*) and SEM (*solid*) computations

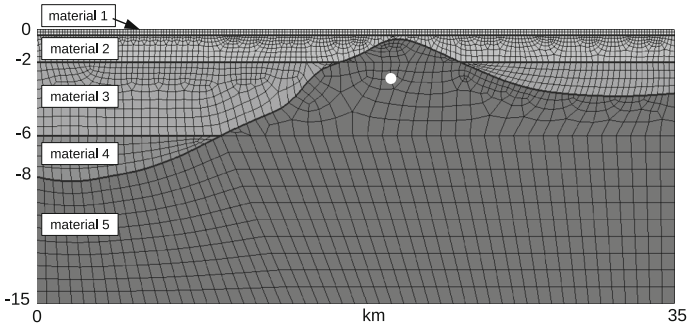

Fig. 6 Unstructured grid for the test case addressed in Sect. 7.4. The mesh spacing varies from $h \approx 150$ m for material 1 to $h \approx 1000$ m for material 5. The source location $\mathbf{x}_s = (19.4, -2.7)$ km is indicated by a *white circle*

7.4 An Application of Geophysical Interest

Since our previous study consists of a rather simple geometry with only one interface, here we construct a more complex situation representing a more realistic application. We consider the computational domain $\Omega = (0, 35) \times (0, -15)$ km shown in Fig. 6, that is a simplified cross-section of the model presented in [40]. The bottom and the lateral boundaries are set far enough from the point source (white dot in Fig. 6) so to avoid any interference of possible reflections from non-perfectly absorbing boundaries with the waves of interest. At the top of the model a free-surface boundary condition is imposed, i.e., $\boldsymbol{\sigma}\mathbf{n} = \mathbf{0}$. We simulate a point source load of the form (49) applied to the point $\mathbf{x}_s = (19.4, -2.7)$ km with unitary amplitude. The computational domain is discretized using an unstructured grid made by 2658 quadrilateral elements, with a mesh size varying from $h \approx 150$ m for material 1 to $h \approx 1000$ m for material 5. The grid spacing is chosen small enough not only to

Table 4 Material properties used for the computational domain in Fig. 6

	$\rho[kg/m^3]$	$\lambda\ [Nm^{-2}]$	$\mu\ [Nm^{-2}]$
Material 1	1800	3.726×10^9	0.162×10^9
Material 2	2000	4.685×10^9	0.720×10^9
Material 3	2100	5.712×10^9	1.344×10^9
Material 4	2200	5.302×10^9	3.168×10^9
Material 5	2300	7.889×10^9	10.14×10^9

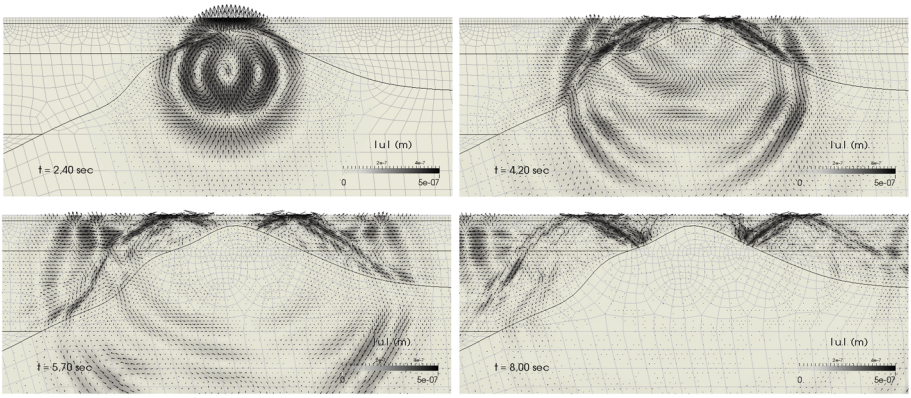

Fig. 7 Snapshots of the computed displacement field $\mathbf{u}$ at different time $t = 2.4, 4.2, 5.7, 8$ s. Due to the material heterogeneities, high oscillations and perturbations of the wave front can be observed. Rayleigh waves moving leftwards and rightwards are clearly visible on the top surface

describe with sufficient precision the physical profile of the submerged topography but also to guarantee in the whole domain at least 5 points per wavelength with polynomial degree equal to 4 and avoid dispersion and dissipation errors, see [4]. We assign constant material properties within each region as described in Table 4. In Fig. 7 we report two snapshots of the solution computed with the SIP method (with $\mathbf{c}_{00} = 10$ and polynomial degree equal to 4) coupled with the leap-frog scheme, fixing the final observation time $T = 10$ s and time step $\Delta t = 1 \cdot 10^{-4}$ s. The discontinuities between the mechanical properties of the materials produce high oscillations and perturbations on the wave front. In particular, due to the stratigraphy of the model two trains of Rayleigh waves are generated on the surface of the model, one moving rightwards and the other traveling leftwards with respect to projection on the top boundary of the source location. All these complex and relevant phenomena are well captured by the proposed method, see Fig. 7. See also [40] for a further discussion.

8 Conclusions

We have introduced a family of semidiscrete (continuous in time) discontinuous Galerkin approximations for a linear elastodynamics problem with mixed boundary conditions. Our presentation and analysis is made in a general setting, considering both *displacement-stress* and *displacement* DG formulations. We have provided a rigorous stability analysis highlighting that (i) in presence of external forces all the DG schemes satisfy optimal *a priori* discrete energy estimates; (ii) in absence of external forces *displacement-stress* formulations

are fully conservative whereas *displacement* formulations dissipate the total discrete energy. The stability estimates are then used to derive optimal *a priori* error estimates in suitable (mesh-dependent) energy norms. The main conclusions of the numerical comparison carried out can be summarized as follows:

(i) all the methods exhibit approximation errors that are of the same order of magnitude;
(ii) *displacement* methods achieve the same accuracy of *displacement-stress* schemes using much (substantially) fewer degrees of freedom.
(iii) the main advantage of using *displacement-stress* methods with respect to *displacement* schemes is that they guarantee the same level of accuracy in both primal and dual variables. In fact, for the latter methods the stress tensor can be recovered only through a post-processing phase resulting in a loss of accuracy in the approximation.
(iv) IP formulations with no extra velocity stabilization exhibit a less sever stability constraint than the schemes proposed in [45,47], at least when the leap-frog time integration scheme is employed.

Acknowledgments Part of this work was carried out during several visits of the second author to the IMATI-CNR of Pavia. She is grateful to the IMATI for the kind hospitality and support. The work of the second author was partially supported by KAUST Grants BAS/1/1636 − 01 − 01 and Pocket ID 1000000193. The first and the third author have been partially supported by the INdAM-GNCS project "Nonstandard numerical methods for geophysics". The first author has been also partially supported by the Italian research grant no. 2015-0182 "PolyNum: Metodi numerici poliedrici per equazioni alle derivate parziali" funded by Fondazione Cariplo and Regione Lombardia.

Compliance with Ethical Standards

Conflicts of interest The authors declare that they have no conflict of interest.

Appendix: Proof of Lemma 1 and Lemma 2

In this appendix we collect the proofs of the auxiliary Lemmas 1 and 2, used in the stability analysis.

Proof (Proof of Lemma 1) The proof goes along the same lines as in the continuous case with subtle modifications to obtain bounds independent of h. Estimate (31) follows from the Cauchy–Schwarz inequality together with the lower bound of the mass density (2). To show estimate (32), we proceed similarly to get

$$\left| \int_0^t \langle \mathbf{c}_{22}\mathbf{g}_\tau, \boldsymbol{\sigma}^h \mathbf{n} \rangle_{\mathcal{F}_h^N} \, d\tau \right| \leq \mathrm{D}_*^{-1/2} \int_0^t \|\mathbf{g}_\tau\|_{1/2,\Gamma_N} \|\mathbf{c}_{22}^{1/2}\boldsymbol{\sigma}^h \mathbf{n}\|_{0,\mathcal{F}_h^N} \, d\tau \ . \tag{50}$$

Next, we notice that for each $t \in [0, T]$, the map $\mathbf{g}(t)$ belongs to $\mathbf{H}^{1/2}(\Gamma_N)$. The inverse trace theorem [1] guarantees that the trace operator has a continuous right inverse operator, say $\mathfrak{T} : \mathbf{H}^{1/2}(\Gamma_N) \longrightarrow \mathbf{H}^1(\Omega)$. Hence, taking into account the scaling of the parameter $\mathbf{c}_{22}$ and using the trace inequality (15) we have

$$\left\| \mathbf{c}_{22}^{1/2}\mathbf{g} \right\|_{0,F}^2 = c_2 h_F k^{-2} \{\mathcal{D}\}^{-1} \|\mathbf{g}\|_{0,F}^2 \lesssim c_2 k^{-2} \mathrm{D}_*^{-1} \|\mathbf{g}\|_{1,K}^2 \quad \forall\, F \in \mathcal{F}_h^N,\, F \subset \partial K \ ,$$

where, with an abuse of notation, we have denoted by $\mathbf{g} = \mathfrak{T}\mathbf{g}$ the extension of $\mathbf{g}$. Summing over all $F \in \mathcal{F}_h^N$ and using the continuity of the operator $\mathfrak{T}$ we get

$$\left\| \mathbf{c}_{22}^{1/2}\mathbf{g}_\tau \right\|_{0,\mathcal{F}_h^N}^2 \lesssim \sum_{K \in \mathcal{T}_h} \mathrm{D}_*^{-1} \|\mathbf{g}_\tau\|_{1,K}^2 = \mathrm{D}_*^{-1} \|\mathbf{g}_\tau\|_{1,\Omega}^2 \lesssim \mathrm{D}_*^{-1} \|\mathbf{g}_\tau\|_{1/2,\Gamma_N}^2 . \tag{51}$$

Substitution of the above estimate in (50) gives (32). To prove (33), we use integration by parts formula (8) with $\mathbf{w} = \mathbf{g}$ and $\mathbf{z} = \mathbf{u}^h$, together with triangle and Jensen' inequality to get

$$\left| \int_0^t \langle \mathbf{g}, \mathbf{u}_\tau^h \rangle_{\mathcal{F}_h^N} \, d\tau \right| \leq \left| \langle \mathbf{g}_0, \mathbf{u}_0^h \rangle_{\mathcal{F}_h^N} \right| + \left| \langle \mathbf{g}, \mathbf{u}^h \rangle_{\mathcal{F}_h^N} \right| + \int_0^t \left| \langle \mathbf{g}_\tau, \mathbf{u}^h \rangle_{\mathcal{F}_h^N} \right| \, d\tau. \tag{52}$$

Therefore, we only need to estimate the inner product $|\langle \mathbf{g}, \mathbf{u}^h \rangle_{\mathcal{F}_h^N}|$, where the first argument could be either $\mathbf{g}_0$, $\mathbf{g}$ or $\mathbf{g}_\tau$. Applying Hölder's inequality, the trace inequality (16) and inequality (17) with $\omega = F \in \mathcal{F}_h^N$ gives

$$\begin{aligned} \left| \int_F \mathbf{g}\mathbf{u}^h ds \right| &\leq \|\mathbf{g}\|_{L^q(F)} \|\mathbf{u}^h\|_{L^p(F)} \lesssim \|\mathbf{g}\|_{L^q(F)} h^{-1/p} \|\mathbf{u}^h\|_{\mathbf{W}^{1,p}(K)} \\ &\lesssim \|\mathbf{g}\|_{L^q(F)} h^{-1/p} h^{d(\frac{1}{p}-\frac{1}{2})} \|\mathbf{u}^h\|_{1,K} = \|\mathbf{g}\|_{L^q(F)} h^{\frac{2d-2-dp}{2p}} \|\mathbf{u}^h\|_{1,K} \, , \end{aligned}$$

where, for any $F \in \mathcal{F}_h^N$, K is the only element in $\mathcal{T}_h$ such that $F \subset \partial K$. Setting now $p = (2d-2)/d$ (whose conjugate is $q = \frac{(2d-2)}{(d-2)}$) the above inequality becomes

$$\left| \int_F \mathbf{g}\mathbf{u}^h ds \right| \lesssim \|\mathbf{g}\|_{L^q(F)} \|\mathbf{u}^h\|_{1,K}. \tag{53}$$

Notice that $q = \infty$ for $d = 2$ and $q = 4$ for $d = 3$. Using that F is a $(d-1)$ dimensional object and using the continuity of the Sobolev embedding $H^1(F) \longrightarrow L^q(F)$, [1], we have

$$\|\mathbf{g}\|_{\mathbf{L}^q(F)} \lesssim \|\mathbf{g}\|_{1,F} \quad \forall \mathbf{g} \in \mathbf{H}^1(F), \quad q = \frac{(2d-2)}{(d-2)}.$$

Substituting the above bound in (53) and summing over all faces $F \in \mathcal{F}_h^N$, gives

$$\left| \langle \mathbf{g}, \mathbf{u}^h \rangle_{\mathcal{F}_h^N} \right| \lesssim \|\mathbf{g}\|_{1,\Gamma_N} \left(\|\mathbf{u}^h\|_{0,\mathcal{T}_h}^2 + \left|\mathbf{u}^h\right|_{1,\mathcal{T}_h}^2 \right)^{1/2}. \tag{54}$$

Applying the discrete Poincaré and Korn inequalities [8,9], and the bound in (5), we have

$$\|\mathbf{u}^h\|_{0,\mathcal{T}_h}^2 + |\mathbf{u}^h|_{1,\mathcal{T}_h}^2 \lesssim \|\boldsymbol{\varepsilon}(\mathbf{u}^h)\|_{0,\mathcal{T}_h}^2 + \sum_{F \in \mathcal{F}_h^o \cup \mathcal{F}_h^D} \left\| h_F^{-1/2} [\![\mathbf{u}^h]\!] \right\|_{0,F}^2 \lesssim \mathrm{D}_*^{-1} \left\| \mathbf{u}^h \right\|_a^2.$$

Finally, substituting the above estimate in (54) yields

$$\left| \langle \mathbf{g}, \mathbf{u}^h \rangle_{\mathcal{F}_h^N} \right| \lesssim \|\mathbf{g}\|_{1,\Gamma_N} \mathrm{D}_*^{-1} \left\| \mathbf{u}^h \right\|_a.$$

Applying now the above estimate to each term in (52), we finally get

$$\begin{aligned} \left| \langle \mathbf{g}_0, \mathbf{u}_0^h \rangle_{\mathcal{F}_h^N} \right| &\lesssim \mathrm{D}_*^{-1} \|\mathbf{g}_0\|_{1,\Gamma_N} \left\| \mathbf{u}_0^h \right\|_a, \\ \int_0^t \left| \langle \mathbf{g}_\tau, \mathbf{u}^h \rangle_{\mathcal{F}_h^N} \right| \, d\tau &\lesssim \int_0^t \mathrm{D}_*^{-1/2} \|\mathbf{g}_\tau\|_{1,\Gamma_N} \left\| \mathbf{u}^h \right\|_a \, d\tau. \\ \left| \langle \mathbf{g}(t), \mathbf{u}^h(t) \rangle_{\mathcal{F}_h^N} \right| &\lesssim \frac{\mathrm{D}_*^{-1}}{\epsilon} \|\mathbf{g}(t)\|_{1,\Gamma_N}^2 + \epsilon \left\| \mathbf{u}^h(t) \right\|_a^2, \end{aligned}$$

where for the last term we have also used the arithmetic geometric inequality with $\epsilon > 0$. Substitution of the above estimates into (52) completes the proof. □

Proof (Proof of Lemma 2) We start rewriting the second equation in (22) with $\boldsymbol{\tau} = \mathcal{D}\boldsymbol{\varepsilon}(\mathbf{u}^h)$

$$\begin{aligned}\|\mathcal{D}^{1/2}\boldsymbol{\varepsilon}(\mathbf{u}^h)\|^2_{0,\mathcal{T}_h} = (\boldsymbol{\varepsilon}(\mathbf{u}^h), \mathcal{D}\boldsymbol{\varepsilon}(\mathbf{u}^h))_{\mathcal{T}_h} = (\mathcal{A}\boldsymbol{\sigma}^h, \mathcal{D}\boldsymbol{\varepsilon}(\mathbf{u}^h))_{\mathcal{T}_h}\\ +\langle \mathbf{c}_{22}[\![\boldsymbol{\sigma}^h]\!], [\![\mathcal{D}\boldsymbol{\varepsilon}(\mathbf{u}^h)]\!]\rangle_{\mathcal{F}_h^o} + \langle \mathbf{c}_{22}(\boldsymbol{\sigma}^h\mathbf{n} - \mathbf{g}), \mathcal{D}\boldsymbol{\varepsilon}(\mathbf{u}^h)\,\mathbf{n}\rangle_{\mathcal{F}_h^N}\\ +\langle [\![\mathbf{u}^h]\!], \{\mathcal{D}\boldsymbol{\varepsilon}(\mathbf{u}^h)\}\rangle_{\mathcal{F}_h^o\cup\mathcal{F}_h^D} - \langle \{\mathbf{u}^h\}_{(1-\delta)} - \{\mathbf{u}^h\}, [\![\mathcal{D}\boldsymbol{\varepsilon}(\mathbf{u}^h)]\!]\rangle_{\mathcal{F}_h^o}, \quad (55)\end{aligned}$$

Prior to estimate all terms on the right-hand side above, we note that Agmon's (14) and inverse inequalities (18), and the definition of $\mathbf{c}_{22}$ give

$$\left\|\mathbf{c}_{22}^{1/2}[\![\mathcal{D}\boldsymbol{\varepsilon}(\mathbf{u}^h)]\!]\right\|_{0,F} \lesssim \|\mathcal{D}^{1/2}\boldsymbol{\varepsilon}(\mathbf{u}^h)\|_{0,K}, \quad \left\|\mathbf{c}_{22}^{1/2}\{\mathcal{D}\boldsymbol{\varepsilon}(\mathbf{u}^h)\}_\delta\right\|_{0,F} \lesssim \|\mathcal{D}^{1/2}\boldsymbol{\varepsilon}(\mathbf{u}^h)\|_{0,K}\,. \quad (56)$$

Using Cauchy–Schwarz inequality and the first estimate above, the first three terms in (55) can be bounded by

$$\begin{aligned}\left|(\mathcal{A}\boldsymbol{\sigma}^h, \mathcal{D}\boldsymbol{\varepsilon}(\mathbf{u}^h))_{\mathcal{T}_h}\right| &\le \|\mathcal{A}^{1/2}\boldsymbol{\sigma}^h\|_{0,\mathcal{T}_h}\|\mathcal{D}^{1/2}\boldsymbol{\varepsilon}(\mathbf{u}^h)\|_{0,\mathcal{T}_h},\\ \left|\langle \mathbf{c}_{22}[\![\boldsymbol{\sigma}^h]\!], [\![\mathcal{D}\boldsymbol{\varepsilon}(\mathbf{u}^h)]\!]\rangle_{\mathcal{F}_h^o}\right| &\lesssim \left\|\mathbf{c}_{22}^{1/2}[\![\boldsymbol{\sigma}^h]\!]\right\|_{0,\mathcal{F}_h^o}\|\mathcal{D}^{1/2}\boldsymbol{\varepsilon}(\mathbf{u}^h)\|_{0,K}\\ \left|\langle \mathbf{c}_{22}(\boldsymbol{\sigma}^h\mathbf{n} - \mathbf{g}), \mathcal{D}\boldsymbol{\varepsilon}(\mathbf{u}^h)\,\mathbf{n}\rangle_{\mathcal{F}_h^N}\right| &\lesssim \left(\|\mathbf{c}_{22}^{1/2}[\![\boldsymbol{\sigma}^h]\!]\|_{0,\mathcal{F}_h^N} + \|\mathbf{c}_{22}^{1/2}\mathbf{g}\|_{0,\mathcal{F}_h^N}\right)\|\mathcal{D}^{1/2}\boldsymbol{\varepsilon}(\mathbf{u}^h)\|_{0,K}.\end{aligned}$$

To estimate the last two terms in (55), notice that $\mathbf{c}_{11}\mathbf{c}_{22} = O(1)$ since,

$$\mathbf{c}_{11}^{-1} = \left(c_1 h_F^{-1}k^2\{\mathcal{D}\}\right)^{-1} = (c_1c_2)^{-1}c_2 h_F k^{-2}\{\mathcal{D}\}^{-1} = (c_1c_2)^{-1}\mathbf{c}_{22}.$$

Then, the Cauchy Schwarz inequality and (56) give for the fourth term

$$\begin{aligned}\left|\langle [\![\mathbf{u}^h]\!], \{\mathcal{D}\boldsymbol{\varepsilon}(\mathbf{u}^h)\}\rangle_{\mathcal{F}_h^o\cup\mathcal{F}_h^D}\right| &\lesssim \left\|\mathbf{c}_{11}^{1/2}[\![\mathbf{u}^h]\!]\right\|_{0,\mathcal{F}_h^o\cup\mathcal{F}_h^D}\ \|\mathbf{c}_{22}^{1/2}\{\mathcal{D}\boldsymbol{\varepsilon}(\mathbf{u}^h)\}\|_{0,\mathcal{F}_h^o\cup\mathcal{F}_h^D}\\ &\lesssim \left\|\mathbf{c}_{11}^{1/2}[\![\mathbf{u}^h]\!]\right\|_{0,\mathcal{F}_h^o\cup\mathcal{F}_h^D}\ \|\mathcal{D}^{1/2}\boldsymbol{\varepsilon}(\mathbf{u}^h)\|_{0,\Omega}.\end{aligned}$$

Analogously, the last term can be estimated using identity (13) and (56)

$$\left|-\langle \{\mathbf{u}^h\}_{(1-\delta)} - \{\mathbf{u}^h\}, [\![\mathcal{D}\boldsymbol{\varepsilon}(\mathbf{u}^h)]\!]\rangle_{\mathcal{F}_h^o}\right| \lesssim \left\|\mathbf{c}_{11}^{1/2}[\![\mathbf{u}^h]\!]\right\|_{0,\mathcal{F}_h^o}\|\mathcal{D}^{1/2}\boldsymbol{\varepsilon}(\mathbf{u}^h)\|_{0,\Omega}.$$

Finally, substituting all the estimates into (55) we obtain

$$\|\mathcal{D}^{1/2}\boldsymbol{\varepsilon}(\mathbf{u}^h)\|_{0,\mathcal{T}_h} \lesssim \|\mathcal{A}^{1/2}\boldsymbol{\sigma}^h\|_{0,\mathcal{T}_h} + \left\|\mathbf{c}_{11}^{1/2}[\![\mathbf{u}^h]\!]\right\|_{0,\mathcal{F}_h^o} + \left\|\mathbf{c}_{22}^{1/2}[\![\boldsymbol{\sigma}^h]\!]\right\|_{0,\mathcal{F}_h^N} + \left\|\mathbf{c}_{22}^{1/2}\mathbf{g}\right\|_{0,\mathcal{F}_h^N},$$

The proof is then concluded by arguing as in the proof of (32) in Lemma 1 (using estimate (51))

$$\left\|\mathbf{c}_{22}^{1/2}\mathbf{g}\right\|^2_{0,\mathcal{F}_h^N} \lesssim \mathrm{D}_*^{-1}\|\mathbf{g}\|^2_{1/2,\Gamma_N}.$$

□

References

1. Adams, R.A., Fournier, J.J.F.: Sobolev Spaces, Volume 140 of Pure and Applied Mathematics, 2nd edn. Elsevier, Amsterdam (2003)

2. Antonietti, P.F., Ayuso de Dios, B., Mazzieri, I., Quarteroni, A.: Stability analysis for discontinuous Galerkin approximations of the elastodynamics problem. Technical Report MOX Report 56/2013, (2013)
3. Antonietti, P.F., Marcati, C., Mazzieri, I., Quarteroni, A.: High order discontinuous Galerkin methods on simplicial elements for the elastodynamics equation. Numer. Algorithms (2015). doi:10.1007/s11075-015-0021-7
4. Antonietti, P.F., Mazzieri, I., Quarteroni, A., Rapetti, F.: Non-conforming high order approximations of the elastodynamics equation. Comput. Methods Appl. Mech. Eng. **209**(212), 212–238 (2012)
5. Arnold, D.N.: An interior penalty finite element method with discontinuous elements. SIAM J. Numer. Anal. **19**(4), 742–760 (1982)
6. Arnold, D.N., Brezzi, F., Cockburn, B., Marini, L.D.: Unified analysis of discontinuous Galerkin methods for elliptic problems. SIAM J. Numer. Anal., **39**(5):1749–1779, 2001/02
7. Arnold, D.N., Brezzi, F., Falk, R.S., Marini, L.D.: Locking-free Reissner–Mindlin elements without reduced integration. Comput. Methods Appl. Mech. Eng. **196**(37–40), 3660–3671 (2007)
8. Brenner, S.: Korn's inequalities for piecewise H^1 vector fields. Math. Comp, pp 1067–1087, (2004)
9. Brenner, S.C.: Poincaré–Friedrichs inequalities for piecewise H^1 functions. SIAM J. Numer. Anal. **41**(1), 306–324 (2003)
10. Carcione, J.M., Kosloff, D., Kosloff, R.: Wave-propagation simulation in an elastic anisotropic (transversely isotropic) solid. Q. J. Mech. Appl. Math. **41**(3), 319–346 (1988)
11. Castillo, P., Cockburn, B., Perugia, I., Schötzau, D.: An a priori error analysis of the local discontinuous Galerkin method for elliptic problems. SIAM J. Numer. Anal **38**(5), 1676–1706 (2000). (electronic)
12. Chaljub, E., Komatitsch, D., Vilotte, J., Capdeville, Y., Valette, B., Festa, G.: Spectral element analysis in seismology. In: Wu, R.-S., Maupin, V. (eds.) Advances in Wave Propagation in Heterogeneous Media, Volume 48 of Advances in Geophysics, pp. 365–419. Elsevier - Academic Press, London, UK (2007)
13. Cheng, Y., Shu, C.-W.: A discontinuous Galerkin finite element method for time dependent partial differential equations with higher order derivatives. Math. Comput. **77**(262), 699–730 (2008)
14. Ciarlet, P.: The Finite Element Method for Elliptic Problems. North-Holland, Amsterdam (1978)
15. Cividini, A., Quarteroni, A., Zampieri, E.: Numerical solution of linear elastic problems by spectral collocation methods. Comput. Methods Appl. Mech. Eng. **104**(1), 49–76 (1993)
16. de la Puente, J., Käser, M., Dumbser, M., Igel, H.: An arbitrary high-order discontinuous Galerkin method for elastic waves on unstructured meshes—iv. Anisotropy. Geophys. J. Int. **169**(3), 1210–1228 (2007)
17. Delcourte, S., Fezoui, L., Glinsky-Olivier, N.: A high-order discontinuous Galerkin method for the seismic wave propagation. In: CANUM 2008, volume 27 of ESAIM Proceedings, pp 70–89. EDP Science, Les Ulis, (2009)
18. Duvaut, G., Lions, J.-L.: Inequalities in mechanics and physics. In: Grundlehren der Mathematischen Wissenschaften. (trans: French by C. W. John), p 219, Springer, Berlin (1976)
19. Faccioli, E., Maggio, F., Paolucci, R., Quarteroni, A.: 2d and 3d elastic wave propagation by a pseudo-spectral domain decomposition method. J. Seismol. **1**(3), 237–251 (1997)
20. Faccioli, E., Maggio, F., Quarteroni, A., Tagliani, A.: Spectral-domain decomposition methods for the solution of acoustic and elastic wave equations. Geophysics **61**(4), 1160–1174 (1996)
21. Georgoulis, E.H., Hall, E., Houston, P.: Discontinuous Galerkin methods for advection-diffusion-reaction problems on anisotropically refined meshes. SIAM J. Sci. Comput., **30**(1):246–271, 2007/08
22. Grote, M., Schneebeli, A., Schötzau, D.: Discontinuous Galerkin finite element method for the wave equation. SIAM J. Numer. Anal. **44**(6), 2408–2431 (2006)
23. Hecht, F.: New development in freefem++. J. Numer. Math. **20**(3–4), 251–265 (2012)
24. Helbig, K.: Handbook of geophysical exploration. In: Helbig, K. (ed.) Foundations of Anisotropy for Exploration Seismics, volume 22 of Handbook of Geophysical Exploration: Seismic Exploration. Pergamon, Oxford (1994)
25. Käser, M., Dumbser, M.: An arbitrary high-order discontinuous Galerkin method for elastic waves on unstructured meshes—I. The two-dimensional isotropic case with external source terms. Geophys. J. Int. **166**(2), 855–877 (2006)
26. Käser, M., Dumbser, M.: A highly accurate discontinuous Galerkin method for complex interfaces between solids and moving fluids. Geophysics **73**(3), T23–T35 (2008)
27. Klin, P., Priolo, E., Seriani, G.: Numerical simulation of seismic wave propagation in realistic 3-D geomodels with a fourier pseudo-spectral method. Geophys. J. Int. **183**(2), 905–922 (2010)
28. Komatitsch, D., Barnes, C., Tromp, J.: Simulation of anisotropic wave propagation based upon a spectral element method. Geophysics **65**(4), 1251–1260 (2000)
29. Komatitsch, D., Ritsema, J., Tromp, J.: The spectral-element method, Beowulf computing, and global seismology. Science **298**(5599), 1737–1742 (2002)
30. Komatitsch, D., Tromp, J.: Introduction to the spectral-element method for 3-D seismic wave propagation. Geophys. J. Int. **139**(3), 806–822 (1999)

31. Komatitsch, D., Vilotte, J.: The spectral-element method: an efficient tool to simulate the seismic response of 2D and 3D geological structures. Bull. Seismol. Soc. Am. **88**(2), 368–392 (1998)
32. Kreiss, H.-O., Oliger, J.: Comparison of accurate methods for the integration of hyperbolic equations. Tellus **24**(3), 199–215 (1972)
33. Makridakis, C.G.: On mixed finite element methods for linear elastodynamics. Numer. Math. **61**(2), 235–260 (1992)
34. Makridakis, C.G.: Finite element approximations of nonlinear elastic waves. Math. Comput. **61**(204), 569–594 (1993)
35. Mazzieri, I., Stupazzini, M., Guidotti, R., Smerzini, C.: Speed: spectral elements in elastodynamics with discontinuous galerkin: a non-conforming approach for 3D multi-scale problems. Int. J. Numer. Meth. Eng. **95**(12), 991–1010 (2013)
36. Mercerat, E., Vilotte, J., Sánchez-Sesma, F.: Triangular spectral-element simulation of two-dimensional elastic wave propagation using unstructured triangular grids. Geophys. J. Int. **166**(2), 679–698 (2006)
37. Mizutani, H., Geller, R.J., Takeuchi, N.: Comparison of accuracy and efficiency of time-domain schemes for calculating synthetic seismograms. Phys. Earth Planet. Inter. **119**(1–2), 75–97 (2000)
38. Moczo, P., Kristek, J., Gális, M., Lis, M.: The Finite-Difference Modelling of Earthquake Motions: Waves and Ruptures. Cambridge University Press, Cambridge (2014)
39. Ortner, C., Süli, E.: Discontinuous Galerkin finite element approximation of nonlinear second-order elliptic and hyperbolic systems. SIAM J. Numer. Anal. **45**(4), 1370–1397 (2007)
40. Paolucci, R., Mazzieri, I., Smerzini, C.: Anatomy of strong ground motion: near-source records and three-dimensional physics-based numerical simulations of the Mw 6.0 2012 May 29 Po Plain earthquake, Italy. Geophys. J. Int. **203**(3), 2001–2020 (2015)
41. Patera, A.: A spectral element method for fluid dynamics: laminar flow in a channel expansion. J. Comp. Phys. **54**, 468–488 (1984)
42. Quarteroni, A.: Numerical Models for Differential Problems, volume 8 of MS&A. Modeling, Simulation and Applications. Springer-Verlag Italia, Milan (2014)
43. Quarteroni, A., Zampieri, E.: Finite element preconditioning for Legendre spectral collocation approximations to elliptic equations and systems. SIAM J. Numer. Anal. **29**(4), 917–936 (1992)
44. Raviart, P.-A., Thomas, J.-M.: Introduction à l'analyse numérique des équations aux dérivées partielles. Collection Mathématiques Appliquées pour la Maîtrise. [Collection of Applied Mathematics for the Master's Degree]. Masson, Paris (1983)
45. Rivière, B., Shaw, S., Wheeler, M.F., Whiteman, J.R.: Discontinuous Galerkin finite element methods for linear elasticity and quasistatic linear viscoelasticity. Numer. Math. **95**(2), 347–376 (2003)
46. Rivière, B., Shaw, S., Whiteman, J.R.: Discontinuous Galerkin finite element methods for dynamic linear solid viscoelasticity problems. Numer. Methods Partial Diff. Equ. **23**(5), 1149–1166 (2007)
47. Rivière, B., Wheeler, M.F.: Discontinuous finite element methods for acoustic and elastic wave problems. In: Current trends in scientific computing (Xi'an, 2002), volume 329 of Contemp. Math., pp 271–282. Amer. Math. Soc., Providence, RI, (2003)
48. Seriani, G., Priolo, E., Pregarz, A.: Modelling waves in anisotropic media by a spectral element method. In: Cohen, G. (ed.) Proceedings of the Third International Conference on Mathematical and Numerical Aspects of Wave Propagation, pp. 289–298. SIAM, Philadephia, PA (1995)
49. Stenberg, R.: Mortaring by a method of J. A. Nitsche. In: Computational mechanics (Buenos Aires, 1998). Centro Internac. Métodos Numér. Ing., Barcelona, (1998)
50. Stupazzini, M., Paolucci, R., Igel, H.: Near-fault earthquake ground-motion simulation in the Grenoble valley by a high-performance spectral element code. Bull. Seismol. Soc. Am. **99**(1), 286–301 (2009)
51. Virieux, J., Calandra, H., Plessix, R.-E.: A review of the spectral, pseudo-spectral, finite-difference and finite-element modelling techniques for geophysical imaging. Geophys. Prospect. **59**(5), 794–813 (2011)
52. Wilcox, L.C., Stadler, G., Burstedde, C., Ghattas, O.: A high-order discontinuous Galerkin method for wave propagation through coupled elastic-acoustic media. J. Comput. Phys. **229**(24), 9373–9396 (2010)
53. Xu, H., Day, S.M., Minster, J.-B.H.: Two-dimensional linear and nonlinear wave propagation in a half-space. Bull. Seismol. Soc. Am. **89**(4), 903–917 (1999)
54. Xu, Y., Shu, C.-W.: Optimal error estimates of the semidiscrete local discontinuous Galerkin methods for high order wave equations. SIAM J. Numer. Anal. **50**(1), 79–104 (2012)